Agricultural and Forest Meteorology 362 (2025) 110376

Contents lists available at ScienceDirect

Agricultural and Forest Meteorology

journal homepage: www.elsevier.com/locate/agrformet

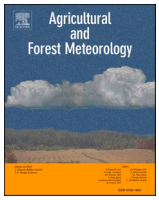

# Crop productivity under heat stress: a structural analysis of light use efficiency models

Peiyu Lai *, Michael Marshall, Roshanak Darvishzadeh, Andrew Nelson

*Faculty of Geo-Information Science and Earth Observation, University of Twente, PO Box 217, 7500 AE, Enschede, the Netherlands*

ARTICLE INFO

*Keywords:*
GPP
Agriculture
Extreme high-temperatures
Climate change
MODIS
Remote sensing

ABSTRACT

The increasing frequency and intensity of extreme heat events necessitate reliable global estimates of crop productivity under heat stress. Light use efficiency (LUE) models are commonly used for macroscale crop productivity estimation but exhibit uncertainties under high-temperature extremes related to the representation of model components and their interactions. They also struggle to isolate heat stress effects from other factors. This study reduced LUE model uncertainty for crop productivity estimation under heat stress by systematically assessing the representations of three essential components: the fraction of photosynthetically active radiation absorbed by the canopy ($F_{PAR}$), the temperature constraint ($F_T$), and the moisture constraint ($F_M$), and the synergy among them under heat-stressed and normal conditions. Model optimizations used data from 75 heat periods (HP) across 18 cropland flux sites worldwide for gross primary production (GPP) estimation, where crops were solely stressed by high temperatures, independent of low soil moisture and unfavorable light. By testing 200 LUE configurations in HP conditions, combing five $F_{PAR}$ and $F_T$ representations, and four $F_M$ representations, we identified the best-performing model, which combined the Enhanced Vegetation Index (EVI)-based $F_{PAR}$, the evaporative fraction (EF)-based $F_M$, and an inverse double exponential $F_T$. This model notably improved GPP estimation under heat stress, comparable to three existing models under normal conditions, further enhancing aboveground biomass estimation across general conditions. Additionally, this study highlighted the limitations of five air temperature-based $F_T$s, while emphasizing the critical contributions of EVI-based $F_{PAR}$ and EF-based $F_M$ under heat stress. These findings emphasize the importance of considering interactions among model components, such as the evapotranspiration effect on $F_T$ and $F_M$, to reduce LUE model uncertainty under extreme conditions. Our findings offer valuable insights for improving crop productivity estimation under heat stress and developing adaptation strategies to mitigate heat stress impacts, thereby ensuring food security in the warming future.

## 1. Introduction

Global warming makes extreme heat events hotter and more frequent during the growing season, leading to crop failure and a decline in global agricultural production (Asseng et al., 2015; Heino et al., 2023; Lobell et al., 2012; Perkins-Kirkpatrick and Lewis, 2020; Zhu et al., 2022). Each 1 °C increase can reduce global yield by 6–10 % (Bras et al., 2021; Lesk et al., 2016; Shew et al., 2020; Zhao et al., 2017). The adverse impact is projected to be more intense and severe under both moderate and severe Representative Concentration Pathways scenarios (RCP 4.5 and RCP 8.5, respectively), threatening future global food security (Becker et al., 2023; Deryng et al., 2014; Meehl and Tebaldi, 2004; Yasin et al., 2022). Given this situation, a reliable estimate of crop productivity under heat stress conditions at the global scale is urgently needed to assess the impact of heat events on global agricultural production and to achieve the Zero Hunger ambitions of SDG-2 (United Nations, 2015).

Gross primary production (GPP) is the rate at which plants capture carbon and convert it to biomass through photosynthesis (Malmstrom et al., 1997). In agroecosystems, GPP is the key determinant of crop productivity, representing the total energy and carbon available for plant growth. By accounting for autotrophic respiration and biomass allocation, GPP enables efficient estimation of dry aboveground biomass (AGB) and crop yield. The light use efficiency (LUE) approach has been widely used for crop productivity estimation at the macroscale because it can be easily parameterized with Earth observation and other gridded geospatial data. The LUE model simplifies photosynthesis to a single “big

* Corresponding author.
*E-mail address:* p.lai@utwente.nl (P. Lai).

https://doi.org/10.1016/j.agrformet.2024.110376
Received 27 August 2024; Received in revised form 18 November 2024; Accepted 19 December 2024
Available online 2 January 2025

leaf", wherein the absorbed photosynthetically active radiation (APAR) is partially converted to organic matter, with a conversion rate defined as LUE (Monteith, 1969). APAR is derived from photosynthetically active radiation (PAR), weighted by the fraction of photosynthetically active radiation absorbed by the canopy ($F_{PAR}$). Therefore, in an ideal situation, GPP is a product of APAR and the potential LUE ($\varepsilon_{max}$). In reality, climate constraints (e.g., temperature and moisture response functions, termed $F_T$ and $F_M$, respectively) are typically used to downregulate GPP further.

Numerous LUE models have been developed, examined, and compared using the big leaf approach to LUE (see reviews by Bao et al. (2022), Jiang et al. (2021), Pei et al. (2022), and Xiao et al. (2019)). In LUE models, heat stress—suppressing photosynthesis by impeding electron transport and carboxylation at temperatures exceeding "optimal" growth conditions (Akter and Islam, 2017; Ristic et al., 2008)—can be captured directly by $F_T$, as well as indirectly by $F_M$ and $F_{PAR}$. The warm-temperature constraint $F_T$ ranging from 0–1, can be represented as a ramp function (Mäkelä et al., 2008; Running et al., 2004) or a parabolic curve (Jarvis et al., 2004; Potter et al., 1993; Raich et al., 1991). The ramp function only considers the positive effect of temperature, resulting in a tendency to overestimate GPP at high temperatures. In contrast, the parabolic $F_T$ curve accounts for heat stress by initially responding positively to temperature increases and then declining beyond the optimal temperature ($T_{opt}$), with some curves falling off more rapidly at high temperatures. Although parabolic $F_T$ curves account for temperature effects, they are parameterized for "normal" growth conditions and may not be suitable for a warming world with increasing frequency, duration, and intensity of heat events (Perkins-Kirkpatrick and Lewis, 2020; Perkins et al., 2012). Additionally, high-temperature extremes can reduce $F_{PAR}$ as plants limit light absorption to avoid excess heat (Tiwari et al., 2020). In the LUE model, $F_{PAR}$ also acts as a latent variable, which accounts for any remaining impacts such as management practices and nutrient availability after considering other environmental constraints (Field, 1991; Garcia et al., 1988). From a model structure perspective, this latent variable also indirectly accounts for temperature effects on light absorption, even though $F_T$ is designed to downregulate $\varepsilon_{max}$ directly. Gitelson et al. (2018) studied soil water stress in maize and soybeans and found similar effectiveness in how $F_{PAR}$ captures water effects; they reported an invariant actual light use efficiency (ε) (i.e., indicating that $F_M$ does not limit LUE) and a substantially reduced $F_{PAR}$. Furthermore, $F_M$ is related to heat stress through water–temperature interactions, as irrigation has been shown to mitigate heat stress in crops such as wheat (Birthal et al., 2021). Thus, heat stress effects in LUE models rely on the combined roles of $F_{PAR}$, $F_T$, and $F_M$.

Parameterizing the above three components has enhanced GPP estimation accuracy. Key advancements include (1) partitioning APAR for sunlit and shaded leaves in multi-leaf LUE models and accounting for diffuse radiation (Donohue et al., 2014; He et al., 2013), (2) estimating $F_{PAR}$ at canopy ($FPAR_{canopy}$) and chlorophyll ($FPAR_{chl}$) levels (Xiao et al., 2004a), and (3) using various moisture indicators to constrain the effect of limited water (Zhang et al., 2015b). Additionally, improvements have been achieved in proxy optimization for components under extreme conditions, such as water-deficit stress (hereafter referred to as "water stress") or combined heat and water stress (i.e., drought). For instance, modifying $F_M$ based on the Normalized Difference Water Index has improved LUE model accuracy in arid and semi-arid grasslands (Ding et al., 2024). However, most model optimization work has been conducted under normal conditions, leaving the capability of existing LUE models to capture heat stress effects on photosynthesis poorly underexplored. Only a few studies have indicated that LUE models' environmental constraints fall short under high-temperature conditions, although they perform well in most situations (Zhao and Zhu, 2023).

Modeling heat effects on GPP is complicated by two main challenges: (1) isolating heat stress effects in natural environments and (2) limited sample sizes in controlled settings. These challenges hinder the validation of current models under extreme heat conditions, integration of satellite observations into $F_T$, and the development of new $F_T$ functional forms. Water and heat stress often happen together in the field and when combined limit crop growth and yield. However, there are important differences in how they impact photosynthesis physiologically and biochemically (Prasad et al., 2008). For instance, under water stress, crops reduce stomatal conductance to prevent water loss, whereas when experiencing heat stress, where water is sufficient, crops increase stomatal conductance to facilitate transpiration and cool leaf temperature (Sadok et al., 2021). More importantly, heat-moisture interactions will likely not be conserved due to climate change (Carter et al., 2016). For example, extremely humid heat events are projected to increase in most crop producing regions (Coffel et al., 2018; Matthews, 2018). If future heat events are more likely to co-occur with high humidity, their interaction effects will differ from historical integrated heat and water deficit stress, e.g., drought (Lesk et al., 2022). Therefore, investigating these combined effects as a unified phenomenon may no longer be sufficient. It is important to investigate LUE model uncertainties under heat stress independently of water stress before exploring their combined effects. In particular, it is essential to assess whether LUE model structures are suitable and capable of accurately reflecting the regulation of all driving factors on GPP and their interactions (Zheng et al., 2018). By optimizing the model structure and the representation of model components (e.g., $F_{PAR}$, $F_T$, and $F_M$) and their synergies under heat stress conditions, the uncertainties of LUE models in crop productivity estimation can be reduced.

This study aims to reduce LUE model uncertainty by accounting for $F_{PAR}$-$F_T$-$F_M$ relations for crop productivity estimation under heat stress conditions. We aim to answer: (1) what is the most sensitive LUE model component under heat and normal conditions, respectively, (2) how do existing LUE models perform under heat conditions, and (3) what are the best component representations and LUE combinations for GPP estimation under heat stress? This study will help improve the LUE model in a warming climate and better understand the impacts of extreme temperatures on agricultural productivity. Based on heat periods identified in prior work (Lai et al., 2024), where photosynthesis was stressed solely by temperatures exceeding $T_{opt}$ for photosynthesis, we first conduct a sensitivity analysis to identify the critical components in LUE models for GPP estimation under different temperature ranges. Then, to enhance the GPP modeling accuracy under heat conditions, we combine different representations of the components to determine the optimal model structure for heat conditions. Finally, the performance of the optimized model in estimating GPP and AGB is compared to that of three commonly used LUE models: the Vegetation Photosynthesis Model (VPM) (Xiao et al., 2004a; Xiao et al., 2004b), the Eddy Covariance-Light Use Efficiency (EC-LUE) model (Yuan et al., 2007), and the Carnegie-Ames-Stanford Approach (CASA) (Potter et al., 1993) model.

## 2. Data and methods

### 2.1. Data

This study used half-hourly flux observations and related meteorological data from 18 cropland sites worldwide (Table 1) as inputs for the LUE models. We obtained flux observations, including latent heat flux (LE), soil heat flux (G), sensible heat flux (H), and GPP derived from the nighttime method (Reichstein et al., 2005) from various regional and international flux networks, including AsiaFlux, FLUXNET, the Integrated Carbon Observation System, and AmeriFlux. These communities calculate GPP using the standardized ONEFlux processing pipeline (Pastorello et al., 2020) using both daytime and nighttime methods. The nighttime method was selected in this study because it results in fewer data gaps than the daytime method. The meteorological dataset consists of air temperature ($T_a$), incoming shortwave radiation (SW_IN), and soil moisture content (SWC). Most half-hourly data were aggregated to the daily timescale by averaging records during the daytime period (filtered

**Table 1**
Summary of the 18 flux tower sites, including locations, data years, crop types, average annual temperature (T), cumulative annual precipitation (PPT), and watering regime.

| Site Code | Site Name | Latitude | Longitude | Country | Site Years | Crop Type | Watering regime | PPT (mm) | T (°C) | Reference |
|---|---|---|---|---|---|---|---|---|---|---|
| US-Ne1 | Mead – Irrigated | 41.1651 | -96.4766 | USA | 2002–2020 | Maize | Irrigated | 790.4 | 10.1 | Suyker et al. (2005) |
| US-Ne2 | Mead – Irrigated Rotation | 41.1649 | -96.4701 | USA | 2002–2020 | Soybean, maize | Irrigated | 788.9 | 10.1 | Suyker and Verma (2012) |
| US-Ne3 | Mead – Rainfed Rotation | 41.1797 | -96.4397 | USA | 2002–2013 | Soybean, maize | Rainfed | 783.7 | 10.1 | Suyker and Verma (2012) |
| US-ARM | Lamont | 36.6058 | -97.4888 | USA | 2002–2011 | Maize, winter wheat | Rainfed | 843 | 14.8 | Bagley et al. (2017) |
| US-CRT | Curtice Walter-Berger | 41.6285 | -83.3471 | USA | 2011–2012 | Soybean | Rainfed | 849 | 10.1 | Lu et al. (2017) |
| US-HRC | Humnoke Farm Field C | 34.5888 | -91.7517 | USA | 2015–2017 | Rice | Irrigated | 1250 | 16.7 | Runkle et al. (2019) |
| US-HRA | Humnoke Farm Field A | 34.5852 | -91.7517 | USA | 2015–2017 | Rice | Irrigated | 1250 | 16.7 | Runkle et al. (2019) |
| FR-Lam | Lamasquere | 43.4965 | 1.2379 | France | 2006–2019 | Maize, winter wheat | Irrigated | 629 | 12.6 | Dare-Idowu et al. (2021) |
| DE-Seh | Selhausen | 50.8706 | 6.4497 | Germany | 2007–2008 | Winter wheat | Rainfed | 693 | 9.9 | Schmidt et al. (2012) |
| IT-Cas | Castellaro | 45.07 | 8.7175 | Italy | 2006–2010 | Rice | Irrigated | 980 | 12.7 | Meijide et al. (2011) |
| IT-BCi | Borgo Cioffi | 40.5237 | 14.9574 | Italy | 2004–2010 | Maize | Irrigated | 600 | 18 | Ranucci et al. (2011) |
| PH-RIF | Philippines Rice Institute | 14.1412 | 121.2653 | Philippines | 2011–2014 | Rice | Irrigated | 2112 | 27.5 | Alberto et al. (2014) |
| KR-CRK | Cheorwon Rice paddy | 38.2013 | 127.2506 | Korea | 2015–2018 | Rice | Irrigated | 1180.9 | 11.2 | Hwang et al. (2020) |
| JP-Mse | Mase Rice paddy | 36.0539 | 140.0267 | Japan | 2002–2006, 2012 | Rice | Irrigated | 1200 | 13.7 | Ouyang et al. (2023) |
| Be-Lon | Lonzee | 50.5516 | 4.7462 | Belgium | 2004–2018 | Sugar beet, potato, winter wheat | Rainfed | 800 | 10 | Aubinet et al. (2009) |
| CH-Oe2 | Oensingen crop | 47.2864 | 7.7337 | Switzerland | 2003–2019 | Pea, winter barley, winter rapeseed, winter wheat | Rainfed | 1155 | 9.8 | Emmel et al. (2018) |
| FR-Gri | Grignon | 48.8442 | 1.9519 | France | 2003–2008, 2011 | Maize, winter barley, winter wheat | Rainfed | 650 | 12 | Loubet et al. (2011) |
| DE-Kli | Klingenberg | 50.8931 | 13.5224 | Germany | 2003–2018 | Maize, winter barley, winter rapeseed, winter wheat | Rainfed | 842 | 7.6 | Prescher et al. (2010) |

by SW_IN > 5 W $m^{-2}$). Maximum daytime values of vapor pressure deficit (VPD) and $T_a$, rather than daily averages, were used for model inputs as plant atmosphere coupling is most pronounced at midday, when eddy formation peaks (Fisher et al., 2008; Marshall et al., 2018).

The flux data were divided into two subsets for analysis. The first dataset comprised half hourly data from 177 growing seasons at 18 flux tower sites and was used to identify heat periods and normal periods, and then the integrated daily data from half hourly data was further used for model optimization with GPP under heat conditions. The second dataset comprised daily data from 23 growing seasons at 3 sites and was used to validate the AGB and GPP estimation under generalized conditions.

The literature identifies heat stress differently (Rezaei et al., 2015). Most studies focus solely on temperature, neglecting other environmental factors such as water availability that can hinder identifying individual contribution of heat stress (Carter et al., 2016). Furthermore, most heat stress identifications mainly originate from climate contexts, neglecting crops' physiological response to heat conditions. In this study, we used a novel heat stress identification method by Lai et al. (2024), which isolates periods where declines in GPP are driven almost exclusively by temperatures surpassing $T_{opt}$ for photosynthesis. The identified heat periods (HP) are isolated from water and light limitations by using a soil physics-based SWC filter accounting for the hysteresis response of photosynthesis. This method is based on half-hourly GPP, SW_IN, $T_a$, and SWC observed from the 18 sites above.

The heat period identification procedure consists of five steps (Fig. 1). It starts by estimating $T_{opt}$ through the GPP-$T_a$ relationship for each crop type grown over multiple years at each site, using the binning technique and the $F_T$ proposed by Potter et al. (1993). Then, in step 2, "Heat Hours" are defined as 30-minute periods during which $T_a$ surpasses $T_{opt}$. If a day has 12 or more such intervals (totaling six hours), it is classified as a "Heat Day." A "Heat Period" is subsequently defined as three or more consecutive heat days. For each possible HP, a normal period (NP) of equal length that precedes the HP within the same growing season is determined. The impact of unfavorable light conditions on GPP is addressed in step 3 to avoid bias in comparisons between heat-stressed and normal crops. This step involves regressing the SW_IN-GPP relationship for HP and NP and calculating the difference between the area under the curve (AUC) for the two regressed curves. A threshold of 1500 umol $CO_2$ $m^{-4}$ $s^{-1}$ W was applied to select samples with a large difference between the AUC of HP and NP, which suggests that the decrease in GPP was unlikely to be attributed to low light conditions. Similarly, step 4 excludes periods of moisture stress using an SWC threshold of 0.25, corresponding to 80 % of field capacity. After these two filters, the final step ensures that HP and NP do not overlap since NP is identified as the period preceding HP. For further details on the heat period identification method, refer to Lai et al. (2024).

75 heat periods were identified from a total of 177 growing seasons at 18 sites, spanning eight crop types: maize (31), rice (13), winter wheat (15), soybean (9), winter barley (4), potato (1), winter rapeseed (1), and pea (1). Further information on the sample set, including the start and end dates of heat periods, site locations, duration, and crop types, are available in Table S1 in the supplementary materials.

Two types of MODIS products were used in this study. The eight-day composited MODIS surface reflectance product (MYD09A1 version 6.1) includes seven bands (Myneni et al., 2021; Roy et al., 2002). Bands 1 (620 - 670 nm), 2 (841- 876 nm), 3 (459 - 479 nm), and 5 (1230–1250 nm) were used to calculate spectral indices, including the Normalized Difference Vegetation Index (NDVI), the Land Surface Water Index (LSWI), and the Enhanced Vegetation Index (EVI). Because of the data gap in MODIS band 6 (1628–1652 nm), we used band 5, which is situated at the boundary of the liquid water absorption, as an alternative for calculating LSWI. The eight-day MODIS $F_{PAR}$ and LAI products (MYD15A2H version 6.1) were also used as inputs for the LUE models (Myneni et al., 2021). To ensure data quality, we excluded records impacted by cloud contamination and other types of noise according to

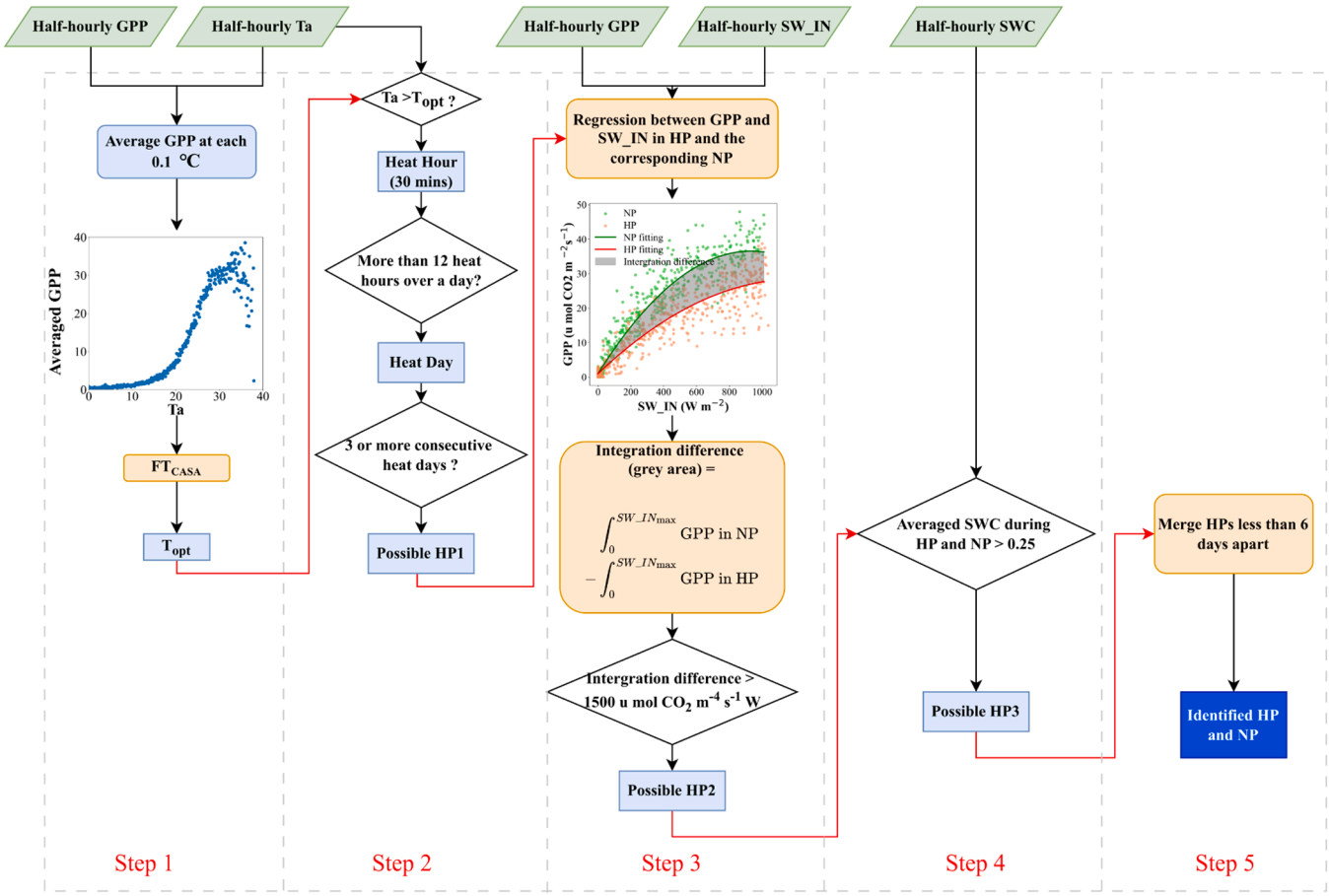


**Fig. 1.** Flowchart for identifying the heat period (HP) and normal period (NP). The equation for $FT_{CASA}$ can be found in Eq E1 in the supplementary materials. Figure modified from Lai et al. (2024).

the accompanying quality control data. Both products have a spatial resolution of 500 m. The MYD09A1 product does not have a consistent temporal resolution of every eight days, as its compositing process selects the observation within eight days, ranking the highest in terms of quality control criteria (Roy et al., 2002). Consequently, the actual observation date for any given eight-day interval varies according to data quality. We followed the criteria proposed by Lai et al. (2024) to select one observation for each HP and NP. For the NP, we prioritized reflectance observations by first selecting the latest observation during the NP, followed by the earliest from the first half of the HP, and finally, the most recent observation before the NP. For the HP, we prioritized the most recent observation from the second half of the HP, followed by the first observation after the HP. Dates of selected observations are listed in Table S1. For the MYD15A2H dataset, the observation representing the eight days that cover the HP or NP was selected.

The AGB estimation and validation used 175 samples from 23 growing seasons for maize and soybean at 3 US sites (US-Ne1, US-Ne2, US-Ne3). The AGB data was obtained from the America AmeriFlux in the Biological, Ancillary, Disturbance, and Metadata (BADM) data (https://ameriflux.lbl.gov/data/badm). AGB was estimated as the cumulative Net Primary Production (NPP) from planting (SOS) to measurement dates, excluding the root section by the root to shoot ratio (RS). The RS values were set to 0.18 for maize and 0.15 for soybean, according to Marshall et al. (2018). NPP was derived from GPP using a 0.53 ratio to account for autotrophic respiration (Yuan et al., 2016).

$$AGB = \sum_{i=sos}^{n} NPP \times \frac{1}{1+RS} \quad (1)$$

## 2.2. Model descriptions

Three widely used LUE models were used for sensitivity analysis and model comparison to inform the "optimal" model structure for heat stress conditions. The VPM model is the first LUE model built upon the conceptual partitioning of photosynthetically active vegetation (PAV) and non-photosynthetically active vegetation (NPV) within the canopy. Only the PAR absorbed by PAV is used for photosynthesis. The fraction of the PAR absorbed by PAV (i.e., green $F_{PAR}$) can be derived from a linear or quadratic function of EVI (Xiao et al., 2004a), which has proven most effective for GPP estimation under heat conditions among several multispectral broadband vegetation indices (VIs) (Lai et al., 2024). Another advantage of the VPM model is its use of the satellite-derived water index LSWI in $F_M$, which is easier to achieve than other water indicators and has been proven more effective than VPD-based $F_M$ under dry conditions (Pei et al., 2020). $F_T$ in VPM is an asymmetric parabolic curve developed for the Terrestrial Ecosystem Model, which was proposed by Raich et al. (1991). This multiplicative approach integrates $F_T$ and $F_M$. Some VPM versions also include a leaf phenology scalar to consider the impact of leaf age on canopy-level photosynthesis (Xiao et al., 2004a). For consistency with the other two models, we used the version described in Xiao et al. (2004b) and Xin et al. (2017), which includes only $F_T$ and $F_M$ as environmental constraints.

Unlike the VPM model, the EC-LUE model only considers the minimum constraint between temperature and water stress, based on Liebig's law of the minimum, i.e., crop growth is determined by the most limiting resource, not by the total amount of available resources (Liebig, 1841). $F_{PAR}$ in the EC-LUE model is based on a linear relationship with NDVI. The $F_T$ in the EC-LUE and VPM models is the same. $F_M$ is proxied

by plant evaporative fraction (EF), as a decrease in energy allocated into latent heat flux indicates a stronger moisture limitation. We used the version described in Yuan et al. (2007).

The CASA model is the first global Production Efficiency Model that uses the big leaf concept (Potter et al., 1993). Initially proposed to estimate net primary productivity, CASA has also been applied to estimate GPP in a different $\varepsilon_{max}$ setting (Chen et al., 2014; Liu et al., 2018). The $F_{PAR}$ in the CASA model relies on the linear relationship with a simple ratio that can be expressed as a transformation of NDVI. The model incorporates two temperature functions to handle both low and high temperature constraints. The high-temperature function is characterized by an asymmetric bell shape that falls off more quickly when $T_a > T_{opt}$ than $T_a < T_{opt}$. The moisture factor in CASA is based on a ratio of actual evapotranspiration ($ET_a$) to potential evapotranspiration ($ET_{opt}$). Both $ET_a$ and $PE_{opt}$ were initially determined using soil moisture models. However, calculating $ET_a$ requires soil depth data and texture-dependent empirical coefficients, which are not consistently available for all sites in this study. Therefore, we adopted the estimation of $ET_a$ with the EC measurement using the approach developed by Priestley and Taylor (1972) and followed by Jiang et al. (2021). Details of model structures and equations for these three models are summarized in Table S2 in the supplementary materials.

All three models used the same PAR and $\varepsilon_{max}$ modeling. PAR was assumed to be a fraction (45 %) of the SW_IN, according to Ma et al. (2014). Models typically treat $\varepsilon_{max}$ as a biome-specific constant. However, its value varies across studies, even for the same crop type, and no universally accepted value exists in the literature (Xin et al., 2017; Yuan et al., 2016). We decided to adjust models to incorporate the metabolism pathway, following the method outlined by Collatz (1991, 1992) to separately estimate $\varepsilon_{max}$ for C3 and C4 crops (Table 2). The key difference between C3 and C4 photosynthesis is how RubisCO delivers and fixes $CO_2$ to produce glucose (Marshall et al., 2023). In C3 plants, RubisCO fixes $CO_2$ directly in the Calvin cycle. However, RubisCO also fixes $O_2$ through photorespiration, which consumes energy and releases $CO_2$ without producing glucose (Gowik et al., 2011). Under high temperatures, RubisCO has a greater affinity to $O_2$ than $CO_2$, leading to increased energy costs related to photorespiration and lower LUE. C4 plants use a different mechanism to concentrate $CO_2$ at the site of RubisCO, thus reducing the oxygenation reaction and photorespiration (Zhu et al., 2010). This adaptation gives C4 plants a comparative advantage (higher LUE), allowing them to maintain relatively higher LUE under elevated temperatures (Morgan et al., 2011).

### 2.3. Sobol sensitivity analysis

Sensitivity analysis helps understand how each uncertainty source contributes to the overall uncertainty. Sobol's sensitivity analysis is a widely used global sensitivity technique that explores the entire input space and accounts for interactions and nonlinear responses among variables (Sobol, 1993). In this study, Sobol's sensitive sensitivity analysis was used to determine the most influential input variables (SW_IN, $T_a$, NDVI, EVI, LSWI, H, LE, and G) in three commonly used LUE models for GPP estimation under low (0 – 20 °C), moderate (20 – 30 °C) and high (30 – 40 °C) temperature conditions. The variable ranges in the sensitivity analysis are shown in Table S3. Sobol's method is variance-based, whereby the variance V of the model prediction is decomposed into partial variances, representing the effects of each input variable and their interactions (Lilburne and Tarantola, 2009),

$$V = \sum_i V_i + \sum_{i<j} V_{ij} + \sum_{j<i<m} V_{ij,m} + \ldots + V_{1,\,2\ldots k} \tag{2}$$

where $V_i$ is the variance attributed to the $i$th input variable, representing the sensitivity of output to $i$th input variable. $V_{ij}$ represents variance explained by the interaction between $i$th and $j$th input variable. $k$ refers to the total number of input variables.

The contribution of the $i$th variable alone, averaged over variations in other variables, is represented by the first-order index $S_i$, also known as the "main effect index". It is standardized by the total variance to provide a fractional contribution.

$$S_i = \frac{Var[E(Y|X_i)]}{Var(Y)} \tag{3}$$

The contribution of the $i$th variable including all variance caused by its interactions of any order, with any other input variables, can be repressed by the total-effect index $S_{Ti}$.

$$S_{Ti} = \frac{E_{X_{\sim i}}\left(Var_{X_i}(Y|X_{\sim i})\right)}{Var(Y)} = 1 - \frac{Var_{X_{\sim i}}\left[E_{X_i}(Y|X_{\sim i})\right]}{Var(Y)} \tag{4}$$

### 2.4. Model optimization

Three different constraints ($F_{PAR}$, $F_T$, and $F_M$) and two model operations for $F_T$ and $F_M$ (multiplicative versus minimum) were combined to develop new LUE models (see Fig. 2). A total of 200 combinations were made, incorporating five $F_{PAR}$ representations, five $F_T$ representations, four $F_M$ expressions, and two model operations to identify the optimal LUE model for estimating GPP under heat stress conditions. These representations include those used in the three existing models, except the $F_M$ expression in the CASA model, which requires soil physical properties data not available in this study. Details are in Fig 3 and Table 3.

### 2.5. Model assessing metrics

We used several indicators to evaluate the performance of the three existing LUE models and the optimized models, compared to the GPP derived from flux observations and the measured AGB: the coefficient of determination ($R^2$), the mean square error (RMSE), and the relative mean square error (RRMSE). These indicators were calculated as follows,

$$R^2 = 1 - \frac{\sum_{i=1}^{n}\left(y_i - y_i^{'}\right)^2}{\sum_{i=1}^{n}\left(y_i - \overline{y}\right)^2} \tag{5}$$

$$RMSE = \sqrt{\sum_{i=1}^{n}\left(y_i - y_i^{'}\right)^2 / n} \tag{6}$$

$$RRMSE = RMSE/\overline{y} \tag{7}$$

where n refers to the number of samples assessed, $y_i$ and $y_i^{'}$ represent observed and estimated GPP (AGB), respectively, and $\overline{y}$ stands for the averaged GPP (AGB) value from flux sites. RRMSE is used to mitigate the impacts of differences in GPP (AGB) distributions during HP and NP.

**Table 2**
Maximum light use efficiency $\varepsilon_{max}$ modeling for C3 and C4 crops based on Collatz (1991; 1992).

| Parameter | Description | Equations |
|---|---|---|
| $\varepsilon_{max,\ C3}$ | $\varepsilon_{max}$ for C3 crops | $55.2 \times \alpha$ g MJ$^{-1}$ |
| $\alpha$ | Quantum yield | $\alpha = 0.08\left(\frac{P_i - \Gamma^*}{P_i + 2\Gamma^*}\right)$ *moles mole*$^{-1}$ |
| $P_i$ | Internal leaf CO2 concentration internal leaf | 23.8 *Pa* |
| $\Gamma$* | CO2 photo compensation point | $\Gamma^* = \frac{[O_2]}{2\tau}$ $[O_2] = 20900$ Pa |
| $\tau$ | The CO2/O2 specificity ratio | $\tau = 2600 \times 0.57\left(\frac{T_a - 20}{10}\right)$ |
| $\varepsilon_{max,\ C4}$ | $\varepsilon_{max}$ for C4 crops | 2.76 g MJ$^{-1}$ |

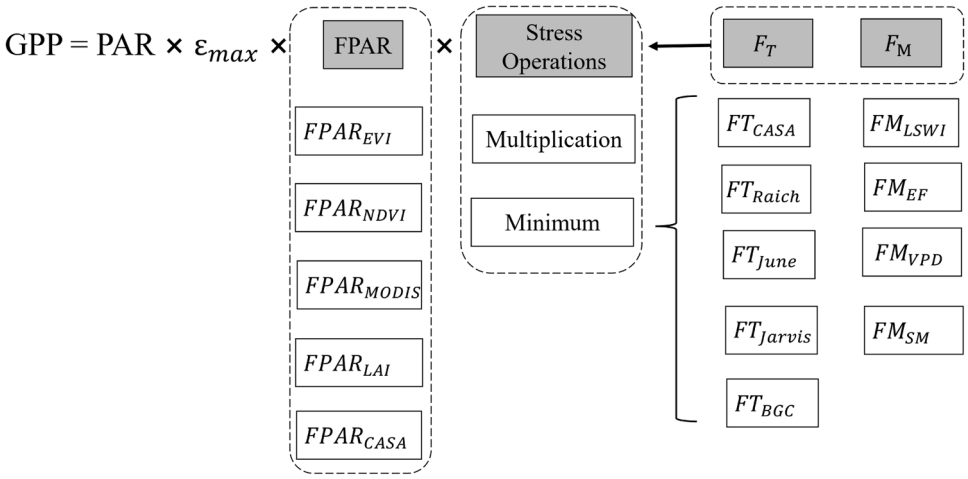


**Fig. 2.** Representations of components ($F_{PAR}$, $F_M$, $F_T$, stressors operation) for LUE model structure. Each component was assigned one representation at a time.

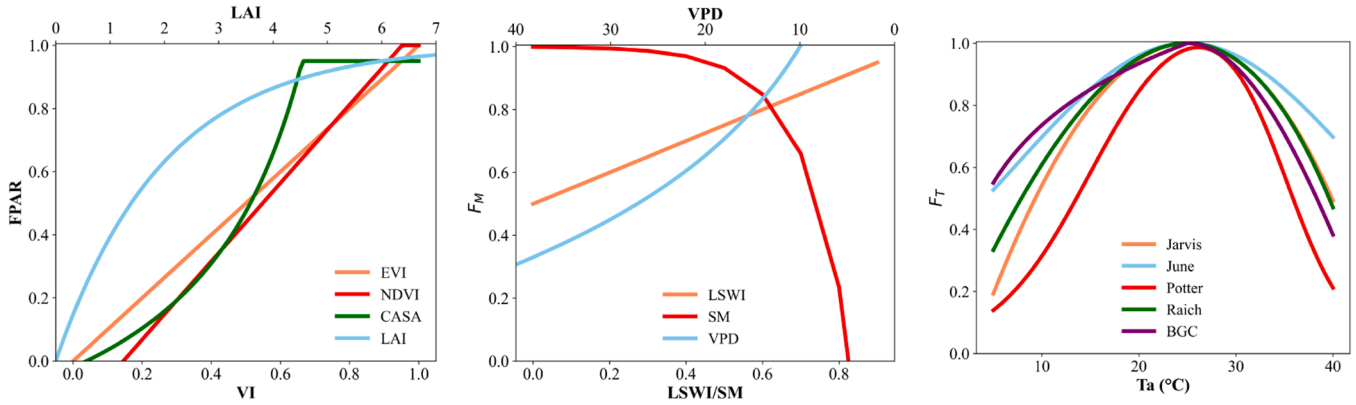


**Fig. 3.** Partial representations for three components of LUE model used in this study: (a) $F_{PAR}$, (b) $F_{M,}$ and (c) $F_T$. VPD is in hPa, and soil moisture content is on a percentile scale. $FPAR_{MODIS}$ and $FM_{EF}$ are not shown here as $FPAR_{MODIS}$ comes from standard products, and $FM_{EF}$ involves multiple variables.

## 3. Results

### 3.1. Sensitivity analysis

Generally, radiation (SW_IN) and indices for estimating $F_{PAR}$ (i.e., EVI and NDVI) show primary sensitivities (Fig. 4a, e, and i). The total order Sobol's index ($S_T$) indicates that VPM is most sensitive to SW_IN, while EC-LUE and CASA are most sensitive to NDVI (Fig. 4a, e, and i). After these two components, $T_a$ also has significant sensitivity across a wide temperature range (0–40°C). However, this sensitivity varies across three temperature ranges (low, moderate, and high). All three models show high sensitivity to $T_a$ at both cool (0–20°C) and warm (30–40°C) conditions but less sensitivity in the optimal range (20–30 °C). Under cool conditions, $T_a$ is the most sensitive input after PAR and $F_{PAR}$ for both VPM and CASA (Fig. 4b and j), with $S_T$ around 0.3, surpassing the sensitivity of variables for $F_M$. However, LE ($F_M$) has slightly more influence than $T_a$ in the EC-LUE model (Fig. 4f). At the optimal temperature range, where most site- and crop-specific $T_{opt}$s fall, all three models exhibit very low sensitivity to $T_a$. The relative weak constraint of $T_a$ in the optimal range increases the contribution of other components, resulting in greater sensitivity to $F_{PAR}$, $F_M$, and radiation in the VPM and EC-LUE models, and enhances the sensitivity of NDVI in the CASA model (Fig. 4k). At high-temperature ranges, sensitivity to $T_a$ increases across all three models. In particular, $T_a$ even surpasses SW_IN and becomes the second most sensitive input in the CASA model (Fig. 4l).

In all three models, $S_1$, which indicates the influences of individual inputs, exhibits similar patterns to $S_T$. The EC-LUE and CASA models show greater differences between $S_T$ and $S_1$ than the VPM model, indicating considerable uncertainties due to interactions between inputs in those two models.

### 3.2. Model optimization and validation

Based on sensitivity analysis indicating that LUE models exhibit varying sensitivity to inputs across different temperature ranges, and informed by crop physiology literature, we chose three important components, $F_{PAR}$, $F_T$, and $F_M$, to optimize the LUE model to improve the GPP estimation under heat conditions. Table 4 shows the 20 best-performing models for GPP estimation under heat and normal conditions. The combination of $FPAR_{EVI}$, $FT_{June}$, $FM_{EF}$, and the multiplicative approach demonstrates superior performance in both HP and NP. Specifically, this combination achieves an $R^2$ of 0.82, an RMSE of 4.8 g C $m^{-2}$ $day^{-1}$, and an RRMSE of 0.21 in HP and relatively lower performance ($R^2$ = 0.70, RMSE = 6.4, RRMSE = 0.28) under NP. Under heat conditions, this combination reduces RMSE by 34 %, 39 %, and 57 % and increases $R^2$ by 9 %, 8 %, and 44 %, compared to the VPM, EC-LUE, and CASA models, respectively.

Under heat conditions, the combination of $FPAR_{EVI}$ and $FM_{EF}$ (Models with IDs 1–10) substantially outperforms other combinations in GPP estimation. Following this, the combination of $FPAR_{EVI}$ and $FM_{LSWI}$, as well as the combination of $FPAR_{NDVI}$ and $FM_{EF}$ have similar performances, with an $R^2$ around 0.75 and RRMSE increasing to 0.35. Notably, performance is mostly the same among the five $F_T$ representations, given the same combination of $F_{PAR}$ and $F_M$ (e.g., model with IDs 1, 2, 4, 8, and 9 in HP).

**Table 3**
Representations for $F_{PAR}$, $F_T$, and $F_M$ used in LUE model combinations. The canopy light extinction coefficient (K) value was assumed to be 0.5 for cropland (Jarvis and Leverenz 1983). Parameters a2 and a3 were set as 0.2 and 0.3, respectively, following Potter et al. (1993), and λ was set to $T_{opt}$ as described by Fisher et al. (2008). $LSWI_{max}$ was set to 1 following Xiao et al. (2004a).

| Representations | Equations | Used in which model | Reference |
|---|---|---|---|
| **FPAR representations** | | | |
| $FPAR_{EVI}$ | $FPAR_{EVI} = EVI$ | VPM | Xiao et al. (2004a) |
| $FPAR_{NDVI}$ | $FPAR_{NDVI} = 1.24 \times NDVI - 0.168$ | EC-LUE | Yuan et al. (2007) |
| $FPAR_{MODIS}$ | MYD15A2H version 6.1 | MODIS GPP product | Myneni et al. (2021) |
| $FPAR_{LAI}$ | $FPAR_{LAI} = 1 - \left(e^{(LAI*(-K))}\right)$ | Lambert–Beer equation | Jarvis and Leverenz (1983) |
| $FPAR_{CASA}$ | $FPAR_{CASA} = \mathrm{Min}\left\{\frac{SR}{SR_{max}-SR_{min}} - \frac{SR_{min}}{SR_{max}-SR_{min}}, 0.95\right\}$ $SR = \frac{1+NDVI}{1-NDVI}$ | CASA | Potter et al. (1993) |
| **FT representations** | | | |
| $FT_{CASA}$ | $FT_{CASA} = FT_{CASA1} \times FT_{CASA2}$ $FT_{CASA1} = 0.8 + 0.02 \times T_{opt} - 0.005 \times {T_{opt}}^2$ $FT_{CASA2} = \frac{1.1814}{\{[1+e^{\alpha 2*(T_{opt}-10-Ta)}] \times [1+e^{\alpha 3*(Ta-10-T_{opt})}]\}}$ | CASA | Potter et al. (1993) |
| $FT_{Raich}$ | $FT_{Raich} = \frac{(T-T_{min})(T-T_{max})}{[(T-T_{min})(T-T_{max})] - (T-T_{opt})^2}$ | VPM, EC-LUE | Raich et al. (1991) |
| $FT_{June}$ | $FT_{June} = e^{\left(-\left(\frac{T-T_{opt}}{\lambda}\right)^2\right)}$ | Model proposed in Fisher et al. (2008) | June et al. (2004) |
| $FT_{Jarvis}$ | $FT_{Jarvis} = \left(\frac{T-T_{min}}{T_{opt}-T_{min}}\right)\left(\frac{T_{max}-T}{T_{max}-T_{opt}}\right)^{\left(\frac{T_{max}-T_{opt}}{T_{opt}-T_{min}}\right)}$ | Model that addressed the effect of temperatures on stomatal conductance. | Jarvis et al. (1997) |
| $FT_{BGC}$ | $FT_{BGC} = \begin{cases} \frac{\log(T+1)}{\log(T_{opt}+1)} & T < T_{opt} \\ \cos\left(\frac{T-T_{opt}}{T_{max}-T_{opt}} \times \frac{\pi}{2}\right) & T \geq T_{opt} \\ 0 & T < 0 \end{cases}$ | Biome-BGC (BioGeochemical Cycles) | Li et al. (2009) |
| **FM representations** | | | |
| $FM_{LSWI}$ | $FM_{LSWI} = \frac{1+LSWI}{1+LSWI_{max}}$ | VPM | Xiao et al. (2004a) |
| $FM_{EF}$ | $FM_{EF} = \frac{LE}{LE+H}$ | EC-LUE | Almeida et al. (2018); Yuan et al. (2007) |
| $FM_{VPD}$ | $FM_{VPD} = 1 - 0.5\ln(VPD)$ | Model that describes the leaf stomatal response to environment changes. | Katul et al. (2009); Medlyn et al. (2011) |
| $FM_{SM}$ | $FM_{SM} = 1 - e^{0.081(SWC-83.3)}$ | 3-PG (Physiological Principles in Predicting Growth) | Pei et al. (2022); Prince and Goward (1995) |

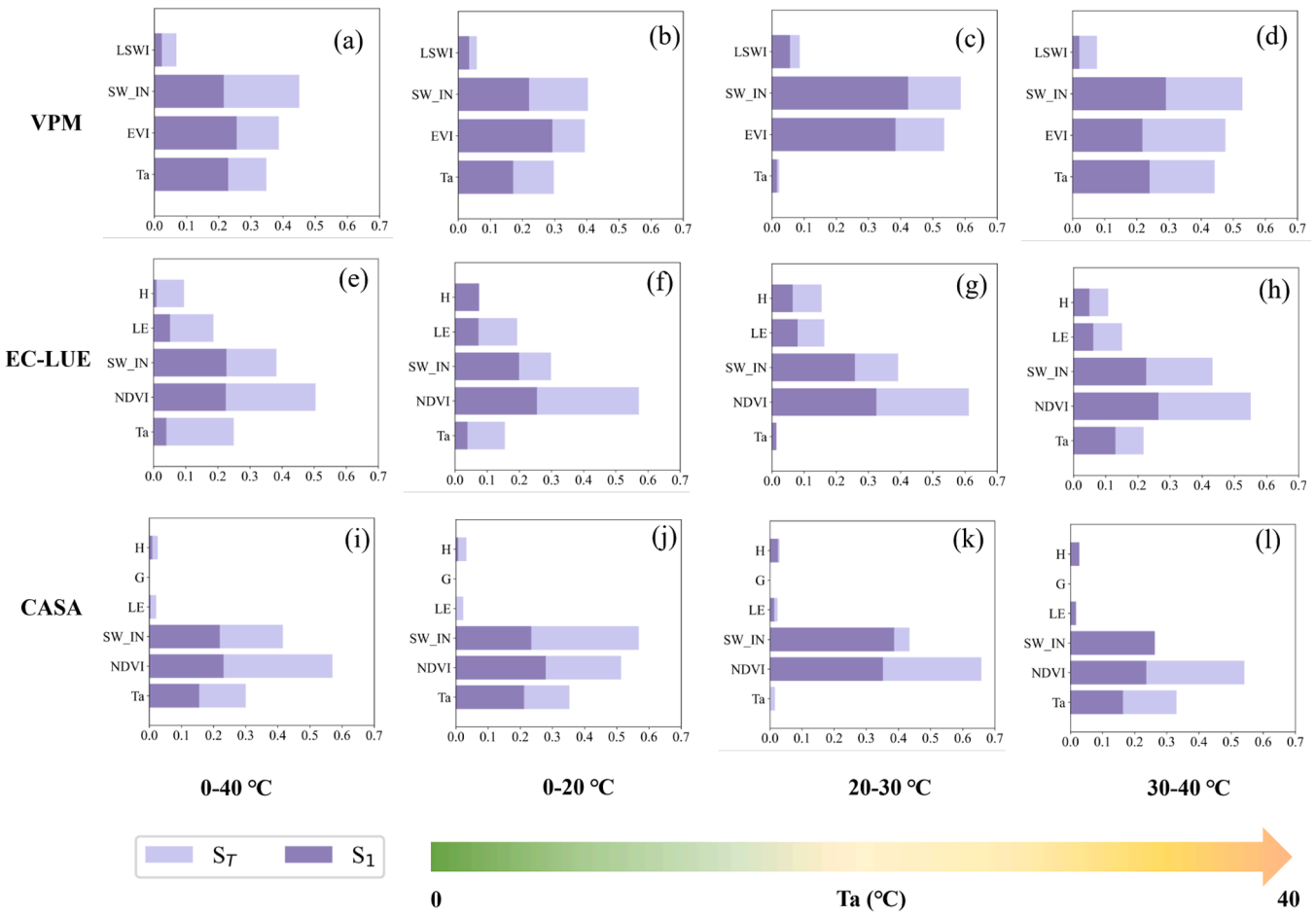


**Fig. 4.** Sobol's first ($S_1$) and total ($S_T$) order indices for sensitivity analysis of VPM, EC-LUE, and CASA models. The first column (a, e, and i) shows the sensitivity across all temperatures, while the next three columns represent cool (0–20°C) (b, f, and j), optimal (20–30°C) (c, g, and k), and warm (30–40°C) (d, h, and l) conditions.

**Table 4**
The top 20 combined LUE models were ordered based on the performance of GPP estimation under heat (HP) and normal (NP) conditions. "×" represents multiplier, "^" represents minimum. The complete table containing all 200 combinations is available in Table S4 in the supplementary materials.

| HP | | | | | | | | NP | | | | | | | |
|---|---|---|---|---|---|---|---|---|---|---|---|---|---|---|---|
| ID | $F_{PAR}$ | $F_T$ | $F_M$ | Operations | $R^2$ | RMSE | RRMSE | ID | $F_{PAR}$ | $F_T$ | $F_M$ | Operations | $R^2$ | RMSE | RRMSE |
| 1 | $FPAR_{EVI}$ | $FT_{June}$ | $FM_{EF}$ | × | 0.821 | 4.834 | 0.213 | 1 | $FPAR_{EVI}$ | $FT_{June}$ | $FM_{EF}$ | × | 0.696 | 6.373 | 0.275 |
| 2 | $FPAR_{EVI}$ | $FT_{Jarvis}$ | $FM_{EF}$ | × | 0.821 | 4.861 | 0.214 | 2 | $FPAR_{EVI}$ | $FT_{BGC}$ | $FM_{EF}$ | × | 0.695 | 6.564 | 0.283 |
| 3 | $FPAR_{EVI}$ | $FT_{June}$ | $FM_{EF}$ | ^ | 0.820 | 4.773 | 0.211 | 3 | $FPAR_{EVI}$ | $FT_{BGC}$ | $FM_{EF}$ | ^ | 0.695 | 6.323 | 0.273 |
| 4 | $FPAR_{EVI}$ | $FT_{Raich}$ | $FM_{EF}$ | × | 0.820 | 4.857 | 0.214 | 4 | $FPAR_{EVI}$ | $FT_{Jarvis}$ | $FM_{EF}$ | × | 0.694 | 6.440 | 0.278 |
| 5 | $FPAR_{EVI}$ | $FT_{Jarvis}$ | $FM_{EF}$ | ^ | 0.820 | 4.783 | 0.211 | 5 | $FPAR_{EVI}$ | $FT_{Jarvis}$ | $FM_{EF}$ | ^ | 0.694 | 6.273 | 0.270 |
| 6 | $FPAR_{EVI}$ | $FT_{Raich}$ | $FM_{EF}$ | ^ | 0.819 | 4.789 | 0.211 | 6 | $FPAR_{EVI}$ | $FT_{June}$ | $FM_{EF}$ | ^ | 0.694 | 6.262 | 0.270 |
| 7 | $FPAR_{EVI}$ | $FT_{BGC}$ | $FM_{EF}$ | ^ | 0.817 | 4.842 | 0.214 | 7 | $FPAR_{EVI}$ | $FT_{Raich}$ | $FM_{EF}$ | ^ | 0.693 | 6.281 | 0.271 |
| 8 | $FPAR_{EVI}$ | $FT_{BGC}$ | $FM_{EF}$ | × | 0.816 | 4.945 | 0.218 | 8 | $FPAR_{EVI}$ | $FT_{Raich}$ | $FM_{EF}$ | × | 0.692 | 6.454 | 0.278 |
| 9 | $FPAR_{EVI}$ | $FT_{CASA}$ | $FM_{EF}$ | × | 0.810 | 5.302 | 0.234 | 9 | $FPAR_{EVI}$ | $FT_{CASA}$ | $FM_{EF}$ | ^ | 0.688 | 6.665 | 0.287 |
| 10 | $FPAR_{EVI}$ | $FT_{CASA}$ | $FM_{EF}$ | ^ | 0.809 | 5.047 | 0.223 | 10 | $FPAR_{EVI}$ | $FT_{CASA}$ | $FM_{EF}$ | × | 0.673 | 7.418 | 0.320 |
| 11 | $FPAR_{NDVI}$ | $FT_{June}$ | $FM_{EF}$ | × | 0.754 | 8.059 | 0.356 | 11 | $FPAR_{LAI}$ | $FT_{BGC}$ | $FM_{EF}$ | × | 0.655 | 5.750 | 0.248 |
| 12 | $FPAR_{NDVI}$ | $FT_{Jarvis}$ | $FM_{EF}$ | × | 0.753 | 8.010 | 0.353 | 12 | $FPAR_{LAI}$ | $FT_{June}$ | $FM_{EF}$ | × | 0.652 | 5.687 | 0.245 |
| 13 | $FPAR_{NDVI}$ | $FT_{Raich}$ | $FM_{EF}$ | × | 0.752 | 8.005 | 0.353 | 13 | $FPAR_{LAI}$ | $FT_{Jarvis}$ | $FM_{EF}$ | × | 0.652 | 5.718 | 0.247 |
| 14 | $FPAR_{NDVI}$ | $FT_{June}$ | $FM_{EF}$ | ^ | 0.752 | 8.134 | 0.359 | 14 | $FPAR_{LAI}$ | $FT_{BGC}$ | $FM_{EF}$ | ^ | 0.650 | 5.636 | 0.243 |
| 15 | $FPAR_{NDVI}$ | $FT_{Jarvis}$ | $FM_{EF}$ | ^ | 0.751 | 8.098 | 0.357 | 15 | $FPAR_{LAI}$ | $FT_{Raich}$ | $FM_{EF}$ | × | 0.649 | 5.729 | 0.247 |
| 16 | $FPAR_{NDVI}$ | $FT_{Raich}$ | $FM_{EF}$ | ^ | 0.751 | 8.082 | 0.357 | 16 | $FPAR_{LAI}$ | $FT_{Raich}$ | $FM_{EF}$ | ^ | 0.648 | 5.646 | 0.243 |
| 17 | $FPAR_{EVI}$ | $FT_{June}$ | $FM_{LSWI}$ | × | 0.750 | 7.138 | 0.315 | 17 | $FPAR_{LAI}$ | $FT_{Jarvis}$ | $FM_{EF}$ | ^ | 0.648 | 5.647 | 0.243 |
| 18 | $FPAR_{EVI}$ | $FT_{Jarvis}$ | $FM_{LSWI}$ | × | 0.749 | 7.176 | 0.317 | 18 | $FPAR_{LAI}$ | $FT_{June}$ | $FM_{EF}$ | ^ | 0.647 | 5.651 | 0.244 |
| 19 | $FPAR_{NDVI}$ | $FT_{BGC}$ | $FM_{EF}$ | × | 0.748 | 7.861 | 0.347 | 19 | $FPAR_{MODIS}$ | $FT_{BGC}$ | $FM_{EF}$ | × | 0.644 | 5.439 | 0.235 |
| 20 | $FPAR_{NDVI}$ | $FT_{BGC}$ | $FM_{EF}$ | ^ | 0.748 | 7.964 | 0.351 | 20 | $FPAR_{MODIS}$ | $FT_{June}$ | $FM_{EF}$ | × | 0.642 | 5.465 | 0.236 |

Under normal conditions, the combination of $FPAR_{EVI}$ and $FM_{EF}$ (Models 1–10) also shows the highest $R^2$ among combinations, but performance is lower than that under heat conditions. However, this combination also exhibits a higher RMSE and RRMSE than models using $FPAR_{LAI}$ or $FPAR_{MODIS}$ combined with $FM_{EF}$ (models 11–20). Similar to HP, $F_T$ does not impact NP performances much (e.g., models 1, 2, 4, 8, and 9 in HP). Additionally, the performances of the $F_T$ and $F_M$ operators were comparable (e.g., models 1 and 3 in HP or models 2 and 3 in NP).

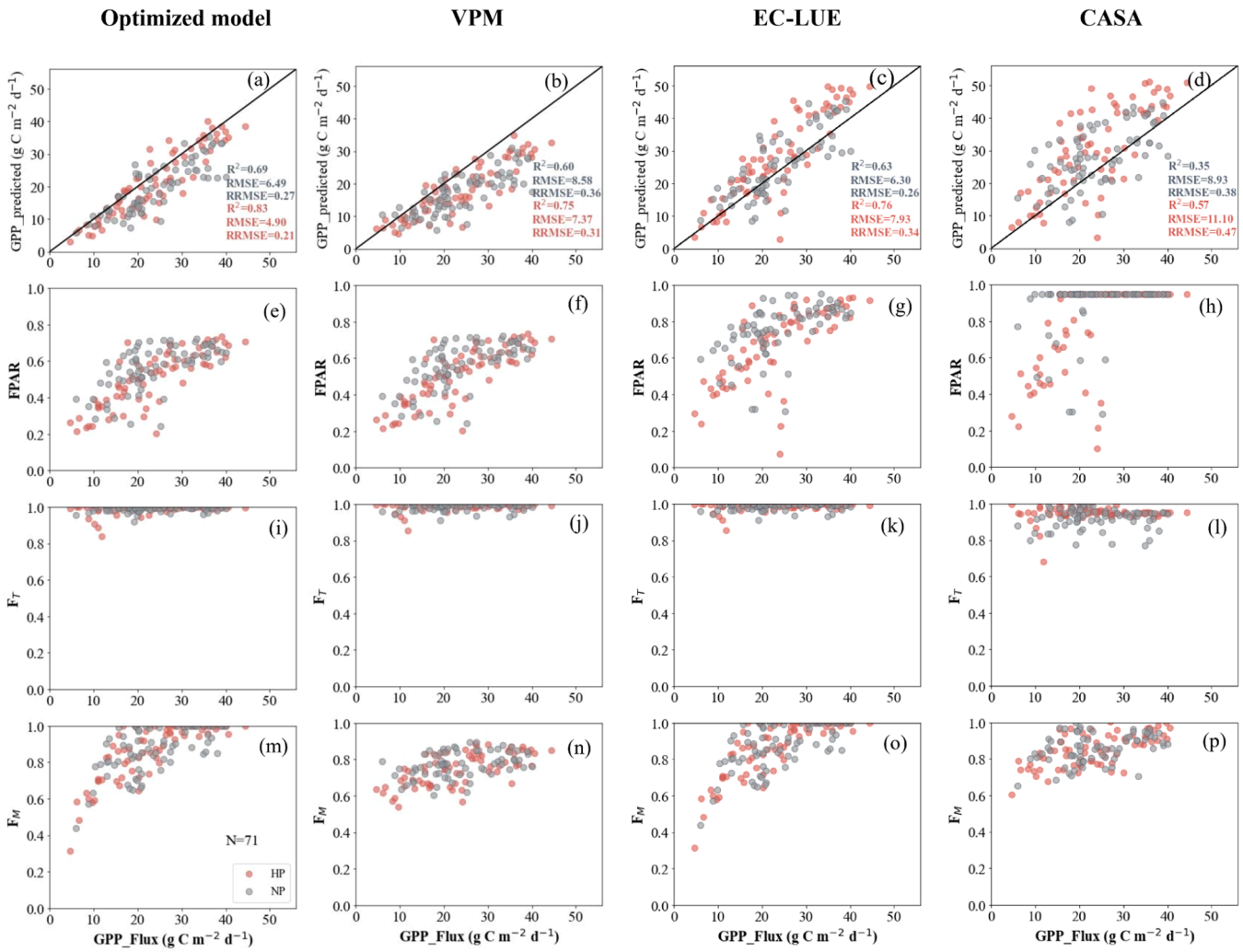


**Fig. 5.** Performance of LUE models (the optimized model, VPM, EC-LUE, and CASA) and their components ($F_{PAR}$, $F_T$, and $F_M$) in estimating GPP under heat (red) and normal (grey) conditions. The sample size (N) indicates that validation was based on 71 samples, limited by the availability of soil flux data for $F_M$ in the CASA model. The optimized model is composed of $FPAR_{EVI}$ (e) $FT_{June}$ (i) and $FM_{EF}$ (m) with the multiplicative approach integrating $F_T$ and $F_M$.

The scatter plots of the best-performing model (i.e., model 1 in Table 4) and its components are shown in Fig. 5 (first columns). The model slightly underestimates GPP (Fig. 5a), especially under normal conditions. $F_{PAR}$ experiences a lower EVI value under heat conditions compared to NP, while no noticeable difference was observed between HP and NP in $F_T$ and $F_M$. Furthermore, $F_{PAR}$ and $F_M$ have a relatively wide range, but $F_T$ is very close to 1, indicating a weak constraint in model building.

The three existing LUE models exhibit lower performance than the best-optimized model (Fig. 5) under heat conditions. The VPM and EC-LUE models show moderate performance with an $R^2$ of nearly 0.76 and RMSE values above 7 (Fig. 5b and c). The CASA model has a lower estimation accuracy due to $F_{PAR}$ saturation (Fig. S1). Under normal conditions, the VPM and EC-LUE models perform similarly to the best-optimized model. However, their performances are much lower than that under heat conditions. The CASA model has a very low $R^2$ and high RMSE in normal conditions.

The VPM model underestimates GPP, especially in NP, due to the relatively lower $F_M$ derived from LSWI (Fig. 5n) and $F_{PAR}$ derived from EVI (Fig. 5f). In contrast, the EC-LUE and CASA models overestimate GPP in both conditions. The overestimating GPP in CASA might be related to the saturation of $F_{PAR}$. Additionally, the relatively high $F_M$ values in the EC-LUE and CASA models compared to VPM contribute to their overestimating GPP. The $FT_{CASA}$ (Fig. 5l) indicates a relatively stronger temperature constraint than the $FT_{Raich}$ (used in VPM and EC-LUE, Fig. 5j and k), but it is still insufficient to counterbalance the overestimation of $F_{PAR}$.

### 3.3. Case study for AGB estimation

To validate the optimized model for general conditions in crop productivity estimating, we used unfiltered data from 23 growing seasons to estimate GPP and AGB. Fig. 6 compares the performance of GPP and AGB estimations from the optimized model and three existing models (VPM, EC-LUE, and CASA). Generally, these models perform similarly across both the 23 growing seasons dataset and the heat and normal periods dataset. VPM tends to underestimate GPP for both maize and soybean, especially at high GPP values. In contrast, the EC-LUE and CASA models overestimate of GPP, while the optimized model provides the most accurate GPP estimates. The optimized model achieves $R^2$ of 0.90 and RMSE of 3.56 g C $m^{-2}$ $day^{-1}$ for maize (Fig. 6a), which is better performed than in HPs and NPs dataset (Fig. 5a). Although the optimized model performs well for maize, it slightly overestimates GPP for soybeans. The improvements are more apparent in RMSE values than in $R^2$. Notably, all four models exhibit better performance for maize than soybean, which could relate to modeling the maximum LUE.

AGB estimation trends align closely with GPP estimation patterns. Over- or under-estimation of GPP typically results in corresponding

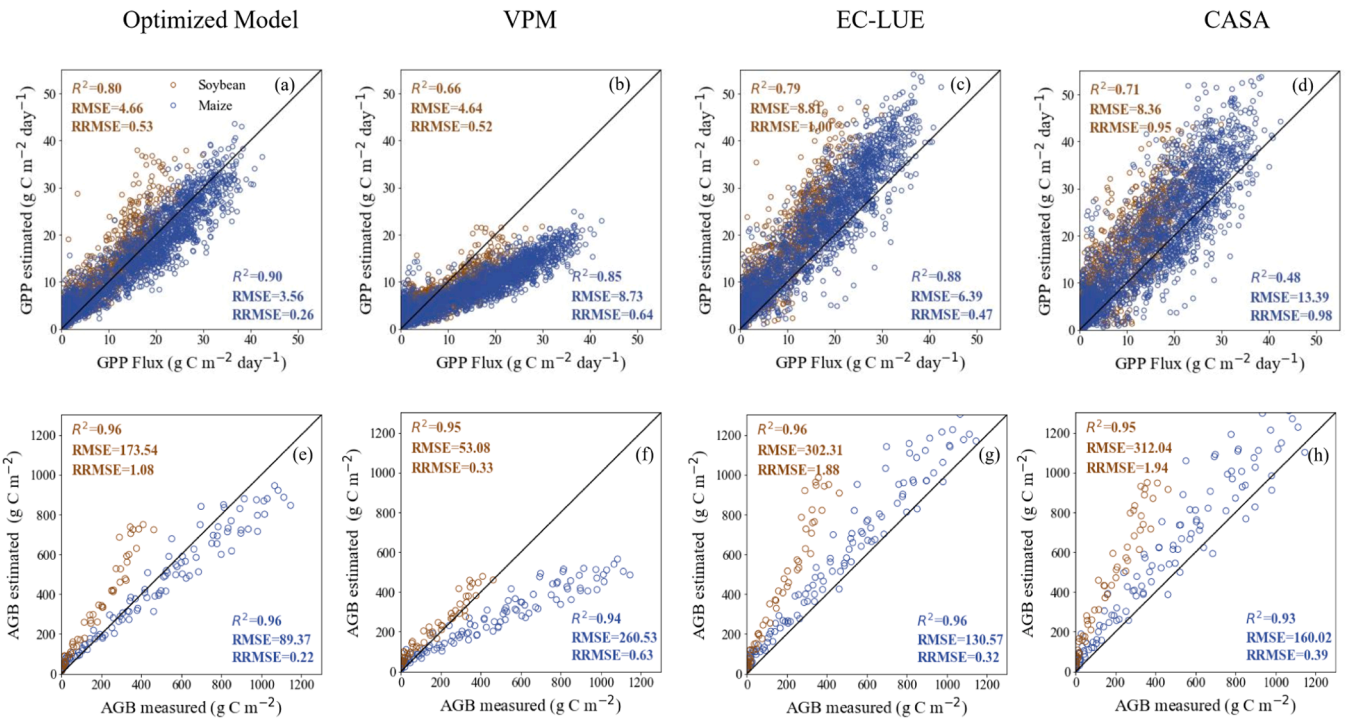


**Fig. 6.** Performance of GPP estimation (top row) and biomass estimation (bottom row) using LUE models (the optimized model, VPM, EC-LUE, and CASA) across 23 growing seasons at 3 US-Ne sites for maize (blue) and soybean (yellow).

biases in AGB estimates. An exception is seen in the VPM model, which underestimates soybean GPP but slightly overestimates soybean AGB. The optimized model improves AGB estimates for maize but overestimates AGB for soybeans. The overestimation of soybean biomass is more pronounced than that of GPP, likely due to the uncertainties in allocating total dry matter to aboveground biomass.

## 4. Discussion

This study revealed considerable variation in GPP estimation under heat conditions, which is attributed to uncertainties in LUE model structures. By analyzing uncertainties in heat periods independent of water and light limitations, we improved the accuracy of GPP estimates under heat conditions and maintained performance comparable to existing models under normal conditions. The estimation of AGB was also improved. The optimal model leverages EVI's strength in representing $F_{PAR}$ and related ε information while also incorporating evapotranspiration to account for the interaction between temperature and water. We have made three key contributions to reduce the uncertainties of crop productivity estimation in the context of warm temperature extremes in a changing climate. First, we found that the warm temperature constraint ($F_T$) is less effective than $F_{PAR}$ in accounting for changes in GPP under heat conditions. Second, EVI-based $F_{PAR}$ enhanced GPP estimation compared to other $F_{PAR}$ representations. Third, incorporating evapotranspiration improved the ability to capture reductions in photosynthesis, further refining GPP and AGB estimation under heat stress.

### 4.1. Model sensitivity under heat conditions

Our study showed that LUE models are more sensitive to PAR and $F_{PAR}$ variables than to $F_T$ and $F_M$, aligning with earlier findings (He et al., 2014; Li et al., 2012; Marshall et al., 2018). On the contrary, Zheng et al. (2018) reported a higher sensitivity of daily minimum temperature than EVI based on Sobol's sensitivity analysis. This discrepancy may be related to the temperature range used for the sensitivity analysis. Our study conducted a sensitivity analysis across three temperature ranges (cool, optimal, and warm) and found that LUE models are sensitive to $T_a$ at high and low temperatures but not at the optimal range (20–30 °C). This aligns with the concept of crop modeling, which incorporates the limiting factors to consider the influence of unfavorable conditions while assuming no constraints under optimal conditions (Jones et al., 2017). The daily minimum temperature referenced in Zheng et al. (2018) likely falls within the low temperature range, similar to our cool conditions (0–20 °C), emphasizing the importance of temperature. This agrees with Wu et al. (2012), who reported that GPP is more sensitive to low temperatures than temperatures around $T_{opt}$. Additionally, Yu et al. (2024) conducted the extended Sobol's Sensitivity Analysis on a two-leaf LUE model. They found $T_a$ to be the most sensitive variable, even more than $F_{PAR}$. This high sensitivity to $T_a$ primarily comes from the interactions beyond Sobol's main effects, which may result from differences in model structure (e.g., involving $F_{PAR}$ for sunlit leaves and shaded leaves) and methodology between their study and ours.

The existing five $F_T$s, and variables involved in these $F_T$s (e.g., $T_a$ and $T_{opt}$) failed to effectively capture heat stress-induced changes in photosynthesis. All five $F_T$ representations showed no discernible difference in GPP estimation with high $F_T$ values, even at the heat extremes. This consistent performance is partly due to their similar representation shapes, unlike $F_{PAR}$ and $F_M$, which exhibit much greater variations (Fig. 2). A commonality analysis on the parameter design of $F_T$ and $F_M$ revealed the general commonality among four existing $F_T$ (including $FT_{CASA}$ and $FT_{Raich}$ used in this study), indicating they generally share similar physical interpretations, whereas the four existing $F_M$ (including $FM_{LSWI}$ and $FM_{EF}$ used in this study) exhibited less commonality (Zhao and Zhu, 2023). This discrepancy is further related to the diversity of indicators used. The distinct characteristics provided by different $F_M$ can be attributed to the varied indicators from atmospheric, soil, and plant water aspects, whereas all four $F_T$ representations rely solely on $T_a$ as an indicator. To our knowledge, no studies have incorporated variables beyond $T_a$ in the $F_T$ component of LUE models, in contrast to the numerous variables used in $F_M$ representing water status. Land surface temperature (LST) has been used in the Temperature and Greenness

(TG) model as a measure of all impacts from temperature, VPD, and PAR, instead of single temperature effects on the physiological activity (Sims et al., 2008). Although LST is closely related to the canopy temperature and VPD, it introduces large uncertainties due to its sensitivity to atmospheric moisture and the hypothesis that LST can represent all climatic conditions does not hold for all ecosystems, suggesting that key climatic variables should be incorporated separately to improve the performance of the TG model (Dong et al., 2017). Given the relationships between LST, temperature, VPD, and the extent of evaporative cooling by vegetation, integrating LST into $F_T$ may enhance the capture of the isolated heat stress effect under conditions of adequate water availability. However, no spectral index has been found to be exclusively related to crop heat status, limiting the incorporation of plants' temperature response into $F_T$ as effectively as the indices (that use the water absorption properties in the short-wave infrared region (SWIR), e.g., LSWI) that are used in $F_M$.

In addition to the representations of $F_T$ and the variables used in $F_T$s, the weak contribution of the five $F_T$s to the LUE models is also related to the sensitivity of photosynthesis to environmental factors and model structure. Both the sensitivity analysis and model optimization revealed that environmental LUE downregulation is less important than $F_{PAR}$ and $\varepsilon_{max}$ (He et al., 2014; Marshall et al., 2018; Yuan et al., 2014). One explanation, provided by a grassland study using the CASA model, is that the formation and degradation of photosynthetic pigments in leaves are closely associated with actual photosynthesis activity, and their variability is primarily captured by $F_{PAR}$ (Bradford et al., 2005). When comparing the contributions of water and temperature constraints, $F_T$ plays a relatively minor role compared to $F_M$ in the LUE model. This is evidenced by models that only consider $F_M$ have fewer errors and greater variations than those that only consider $F_T$ (Yuan et al., 2014). Our study underscored the dominant role of $F_{PAR}$ over environmental constraints (i.e., $F_T$) under heat stress, which is consistent with the findings of Gitelson et al. (2024), which indicated greater variation of $F_{PAR}$ than the downregulated ε by environment constraint (i.e., $F_M$) in water stress. Based on these findings, we suggest that there is more to be gained from further studies on $F_{PAR}$ rather than $F_T$ to enhance the LUE model by accurately capturing the high temperature effects.

Our results highlighted the important impact of the interactions between model inputs (the difference between $S_T$ and $S_1$), which account for nearly half of the uncertainties. Yu et al. (2024) demonstrated that these interactions have a predominant influence over the main Sobol's effect in a two-leaf LUE model. However, He et al. (2014) reported a much smaller difference between $S_T$ and $S_1$ on the VPM model. Further investigation into these variable interactions under diverse extreme environments and biomes is necessary to better understand the uncertainties in LUE models.

### 4.2. Uncertainties in LUE Model Structures

Model structures (i.e., different representations of $F_{PAR}$ and environmental factors as well as the method of integrating them) introduce substantial uncertainty in GPP estimates using the LUE concept. There is ongoing disagreement regarding the relative effectiveness of different representations within each model structure (Yuan et al., 2014).

EVI most accurately represented $F_{PAR}$ among the five $F_{PAR}$ representations. The improved estimation of GPP using EVI can be explained by the accurate representation of $F_{PAR}$, i.e., the concept of $FPAR_{chl}$ and the fewer impacts from soil background. Theoretically, only $FPAR_{chl}$ can be used for vegetation photosynthesis. Scaled EVI has been demonstrated to improve GPP estimation in croplands due to its strong correlation with $FPAR_{chl}$ (Liu et al., 2017), effectively excluding non-photosynthetic components within the canopy. Previous studies have shown that EVI-based $FPAR_{chl}$ estimates GPP more accurately than $FPAR_{canopy}$ derived from NDVI (Cheng et al., 2014), which also explains why $FPAR_{EVI}$ performs better than $FPAR_{NDVI}$ in this study. Additionally, models using $FPAR_{EVI}$ perform very well under heat stress, as EVI not only represents $F_{PAR}$ but also captures variations beyond $F_{PAR}$. For instance, moderate to strong correlations between EVI and ε have been reported in forest sites (Ma et al., 2014; Sims et al., 2006; Wu et al., 2012). Moreover, $T_{opt}$ derived from EVI has been shown to improve the GPP estimation by providing better temperature constraints on ε (Chang et al., 2021). These studies indicate that, in addition to capturing variations in $F_{PAR}$, EVI serves as a latent variable that captures the effects of phenological stage and environmental factors after accounting for $F_T$, $F_M$, and ε, which may improve GPP estimation under heat stress.

$FPAR_{NDVI}$ was the second-best representation under heat conditions. Although NDVI has a nearly linear relationship with $F_{PAR}$ during the growing seasons, it saturates at high LAI values and is sensitive to soil background (Olofsson and Eklundh, 2007). Previous studies have shown that EVI has a closer relationship with GPP than NDVI (Xiao et al., 2004a; Xiao et al., 2005; Xiao et al., 2004b). However, under normal conditions, $FPAR_{LAI}$ (ID 11–18 for NP in Table 4) was the second-best representation of $F_{PAR}$. Models with $FPAR_{LAI}$ have a lower RMSE than those with $FPAR_{EVI}$ in normal conditions, indicating a decline in the effectiveness of $FPAR_{LAI}$ under heat conditions. This decline is likely due to heat-induced changes in canopy structure and light absorption, which alters the relationship between LAI and $F_{PAR}$. For instance, crops can adjust their canopy architecture under high temperatures to optimize light capture and minimize thermal stress, affecting leaf self-shading and LAI, as well as light absorption (Moore et al., 2021). As for $FPAR_{MODIS}$, our results show higher values than $FPAR_{EVI}$, consistent with validation studies that indicate an 8–20 % overestimation in the MODIS $F_{PAR}$ product (Fensholt et al., 2004). MODIS $F_{PAR}$ products are known to suffer from contamination due to cloud cover and extended periods of darkness, especially in high latitudes with low solar angles, where most of our sites are located (Myneni et al., 2002).

The multiplicative and minimum operations between $F_T$ and $F_M$ showed no discernible difference, primarily due to the high $F_T$ values. Mathematically, as $F_T$ values approach 1, the multiplicative and minimum between $F_T$ and $F_M$ converge toward $F_M$, resulting in negligible differences in GPP estimation. The multiplicative approach assumes that the environmental factors are independent, which is inaccurate for $F_T$ and $F_M$ as the strong interactions between water and temperature, especially under extreme conditions. Previous studies highlight that the minimum approach integrating $F_T$ and $F_M$ provides a more accurate representation of the joint effects of temperature and water availability on GPP compared to the multiplicative method (Jiang et al., 2021; Zhang et al., 2015a). Since both $F_T$ and $F_M$ range from 0 to 1, their multiplication is smaller than either $F_T$ or $F_M$, further magnifying the down-regulating effect of environmental factors and leading to an underestimation of GPP (Horn and Schulz, 2011; Jiang et al., 2021). Moreover, the multiplicative and minimum operations can be combined when there are three or more constraints (e.g., min ($F_M$, $F_{CO2}$) × $F_T$), as demonstrated by Yu et al. (2024). Further investigation is required to better understand and model the interactions between these constraints, given effective representations of these climatic factors.

Validation using the unfiltered growing season dataset indicates that LUE models tend to overestimate GPP and AGB for soybeans more than for maize. This variation in performance by crop types may be related to the maximum light use efficiency $\varepsilon_{max}$ and the biomass allocation ratio for AGB. The $\varepsilon_{max}$ estimation is based on the photosynthesis path. C4 crops like maize have a constant $\varepsilon_{max}$ value, while C3 crops exhibit variability with $T_a$. Since all four models used the same $\varepsilon_{max}$ estimation and overestimated AGB for soybean, we suspect this overestimation of AGB is related to the overestimation of $\varepsilon_{max}$, which can be specified by crop type in certain crop models. Additionally, uncertainties in root-to-shoot ratio parameters may further contribute to the differences in model performance between crop types.

### 4.3. The role of evapotranspiration

Isolating heat stress from water stress allows us to reveal the physiological response of crops under high temperatures. Incorporating evapotranspiration into the LUE model enhanced the accuracy of GPP estimation under heat stress, as evidenced by the superior performance of $FM_{EF}$ compared to $F_M$ derived from LSWI, SWC, and VPD. Water stress proxies in LUE models typically include atmospheric indicators (e.g., VPD and RH), soil water indicators (e.g., SWC), or plant water indicators (e.g., EF and LSWI) (Pei et al., 2022). Plant water indicators more accurately represent changes in vegetation water than atmospheric and soil water indicators because they are more sensitive to fluctuations in leaf water content (Zhang et al., 2015b). Under high temperature conditions, crops increase evapotranspiration to cool down, resulting in an increased amount of energy used to evaporate water from plants and soil, i.e., LE (Prasad et al., 2008). $FM_{EF}$ captures the variation of evaporative fraction (LE), thereby minimizing the uncertainty for GPP estimation under heat stress. Originally, $FM_{EF}$ was designed to capture water stress by reflecting a decrease in LE, which indicates reduced evapotranspiration due to stomatal closure under water-limited conditions (Yuan et al., 2007). It effectively captures the interaction between temperature and water, making it a reliable indicator for heat stress when water is sufficient.

The increase of LE confirms the decoupling between photosynthesis and stomatal conductance under heat extremes, where the photosynthesis reduced while the transpiration increased, as shown by experiments carried out in well-watered heat stress environments (Ameye et al., 2012; Urban et al., 2017). This decoupling is found to be dependent upon water availability, i.e., LE increases when water is sufficient and decreases when water supply is limited (De Kauwe et al., 2019). These distinct changes may enhance model performance under extreme conditions, although current crop and land surface models have not decoupled transpiration from the downregulation of photosynthesis with increasing temperature. Given the different responses of crop evapotranspiration to heat (increasing) and water (decreasing) stress, the evaporative fraction might serve as a general environment constraint, potentially replacing $F_T$ and $F_M$. However, this hypothesis needs further testing and analysis through controlled environmental experiments to better understand the interactions between photosynthesis and evapotranspiration under water stress, heat stress, and compound water and heat stress.

Our results provided new evidence on interactions between climatic factors in regulating photosynthesis, as reflected by the sensitivity analysis and the outperformance of $FM_{EF}$. Although these interaction effects are crucial for LUE model development, especially under extreme heat conditions, they have received less attention than the relative importance of each factor individually (Pei et al., 2022). On the one hand, the complex water-temperature interaction on LUE models has only been compared in literature with multiplicative and minimum operations between $F_T$ and $F_M$, as we discussed in section 4.2. On the other hand, incorporating additional factors such as $CO_2$, cloud cover, and vegetation age would introduce further interactions, which could amplify and complicate uncertainties (Cheng et al., 2023). Interactions occur not only among these constraint factors but also between the constraint factors and essential fixed components, such as $F_{PAR}$. To our knowledge, the uncertainties arising from these interactions have not been extensively studied in LUE models, where environmental stressors are often assumed to be independent, potentially leading to parameterization errors. More attention and effort are indeed required to assess uncertainties from variable interactions, especially under extreme climate conditions.

### 4.4. Limitations and future work

This study has several limitations that need to be acknowledged. First, due to the data gap in MODIS bands 6 (1628–1652 nm), band 5 (1230–1250 nm), which is situated at the boundary of the liquid water absorption, was used for LSWI calculation. The lower representation of band 5 of water absorption might reduce the representation of LSWI to plant water variations, introducing uncertainty in GPP estimates. We chose MODIS as the Earth observation data source because a number of heat events could be captured with MODIS's more than 20-year-long record of the Earth's surface. Further investigation can expect better spectral representations of $F_{PAR}$ and climate constraints with MODIS and Sentinel-3 harmonization, which provides better data availability with more heat period samples over the longer term to enhance crop productivity under heat stress. Second, although the model structure was analyzed by combining different components, the parameters for these components were not calibrated in this study due to the limited sample size. For instance, the slope and intercept between $F_{PAR}$ and NDVI in $FPAR_{NDVI}$ were initially designed for forests and may not be suitable for croplands. Future work can calibrate these parameters based on our optimized model using extensive field data specific to different biomes or environmental conditions.

Our study highlights the crucial roles of EVI and evapotranspiration while revealing the limited effectiveness of current $F_T$ under heat stress. These findings offer valuable insights into the interconnections among components within LUE models and suggest pathways for optimizing these models to handle more extreme environments in the future. Notably, accurately estimating $F_{PAR}$ may prove more effective than refining $F_T$ representation. Temperature indicators, rather than the $F_T$ function form itself, could contribute more to improving the representation of temperature effects. For instance, incorporating new spectral-based temperature indicators or evaporative indicators could improve the representation of LUE components. Our previous work attempted to identify such a vegetation index to better capture the heat effect in $F_T$ but was limited by the available spectral observations under heat conditions (Lai et al., 2024). However, these limitations may be overcome by using data from upcoming missions, such as the NIR and SWIR bands in Sentinel 3, and narrow bands in hyperspectral missions, e.g., CHIME, PRISMA, and EnMAP. Linking spectral features in these narrow bands with heat-induced alterations in biophysics and ecophysiology could enhance $F_{PAR}$, $F_M$, and $F_T$ representations in LUE models, leading to a more accurate estimation of global agricultural production (crop area × yield) using Earth observation data.

Moreover, isolating heat stress from water stress allows us to reveal the vital role of physiological response (evapotranspiration) in heat stress. This provides insights into the holistic interaction between environmental constraints (water, $CO_2$, and temperature) that impact the stomatal behavior of plants and photosynthesis and modeling the interactive effects. This approach of identifying and isolating the heat stress period can be transferred to other ecosystems for heat stress investigations. These understandings and implications will be crucial for developing adaptation strategies to mitigate the impacts of increasingly intense and frequent heat events on food security.

## 5. Conclusion

Accurate estimation of crop productivity under extremely high temperatures is urgently needed to safeguard food security under climate change. LUE models are commonly used for macroscale crop yield estimation because they are readily parameterized with Earth observation and geospatial information. However, current LUE models face uncertainties under such conditions, particularly in representing $F_{PAR}$, $F_M$, $F_T$, and their interactions. Our study using 75 heat periods independent of water and light limitations demonstrates that five traditional $F_T$s, based solely on air temperature, are insufficient to capture heat effects. In contrast, EVI-based $F_{PAR}$ and EF-based $F_M$ effectively compensate for the $F_T$ function in improving model performance by capturing changes in $F_{PAR}$, LUE, and evapotranspiration under high temperatures. The isolation of heat stress from water stress reveals the vital role of physiological response (evapotranspiration) in heat

stress. The optimal LUE model, composed of $FPAR_{EVI}$, $FM_{EF}$, and $FT_{June}$ improved GPP estimation under heat stress by reducing RMSE by 34 %, 39 %, and 57 % and increasing $R^2$ by 9 %, 8 %, and 44 %, compared to the VPM, EC-LUE, and CASA models respectively. The optimized model also enhanced GPP estimation under normal conditions, demonstrating its generalizability across a wide temperature range. These advancements also enhanced aboveground biomass estimation for maize. These findings have implications for optimizing crop models under climate change, understanding interactions between water and temperature on photosynthesis, and improving crop productivity estimation at a large scale to support global food security under changing climate.

## CRediT authorship contribution statement

**Peiyu Lai:** Writing – original draft, Visualization, Validation, Software, Methodology, Investigation, Formal analysis, Data curation. **Michael Marshall:** Writing – review & editing, Visualization, Supervision, Resources, Methodology, Conceptualization. **Roshanak Darvishzadeh:** Writing – review & editing, Supervision, Methodology, Conceptualization. **Andrew Nelson:** Writing – review & editing, Supervision, Resources, Project administration, Funding acquisition.

## Declaration of competing interest

The authors declare that they have no known competing financial interests or personal relationships that could have appeared to influence the work reported in this paper.

## Acknowledgements

The work was funded by the China Scholarship Council (CSC) under Grant 202106990015. We extend our gratitude to Dr. Youngryel Ryu, Dr. Minseok Kang, Dr. Tiphaine Tallec, Dr. Aurore Brut, and Dr. Andy Suyker for their valuable assistance in providing the agricultural management data for sites KR-CRK, FR-Lam, US-Ne1, US-Ne2 and US-Ne3. We also thank Dr. Danyang Yu for his technical support in the sensitivity analysis and two anonymous reviewers for their valuable comments that helped improve this study.

## Supplementary materials

Supplementary material associated with this article can be found, in the online version, at doi:10.1016/j.agrformet.2024.110376.

## Data availability

Data will be made available on request.

## References

Akter, N., Islam, M.R., 2017. Heat Stress Effects and Management in Wheat. A review. Agronomy for Sustainable Development, p. 37.
Alberto, M.C.R., Wassmann, R., Buresh, R.J., Quilty, J.R., Correa, T.Q., Sandro, J.M., et al., 2014. Measuring methane flux from irrigated rice fields by eddy covariance method using open-path gas analyzer. Field. Crops. Res. 160, 12–21.
Almeida, C.T.d., Delgado, R.C., Galvão, L.S., Aragão, L.E.d.O.C.e., Ramos, M.C., 2018. Improvements of the MODIS Gross Primary Productivity model based on a comprehensive uncertainty assessment over the Brazilian Amazonia. ISPRS J. Photogram. Remote Sens. 145, 268–283.
Ameye, M., Wertin, T.M., Bauweraerts, I., McGuire, M.A., Teskey, R.O., Steppe, K., 2012. The effect of induced heat waves on inus taeda and uercus rubra seedlings in ambient and elevated CO2 atmospheres. New. Phytol. 196, 448–461.
Asseng, S., Ewert, F., Martre, P., Rotter, R.P., Lobell, D.B., Cammarano, D., et al., 2015. Rising temperatures reduce global wheat production. Nat. Clim. Chang. 5, 143–147.
Aubinet, M., Moureaux, C., Bodson, B., Dufranne, D., Heinesch, B., Suleau, M., et al., 2009. Carbon sequestration by a crop over a 4-year sugar beet/winter wheat/seed potato/winter wheat rotation cycle. Agr. Forest. Meteorol. 149, 407–418.
Bagley, J.E., Kueppers, L.M., Billesbach, D.P., Williams, I.N., Biraud, S.C., Torn, M.S., 2017. The influence of land cover on surface energy partitioning and evaporative fraction regimes in the U.S. Southern Great Plains. J. Geophys. Res.: Atmos. 122, 5793–5807.
Bao, S.N., Wutzler, T., Koirala, S., Cuntz, M., Ibrom, A., Besnard, S., et al., 2022. Environment-sensitivity functions for gross primary productivity in light use efficiency models. Agr. Forest. Meteorol. 312.
Becker, R., Schüth, C., Merz, R., Khaliq, T., Usman, M., Beek, T.a.d., et al., 2023. Increased heat stress reduces future yields of three major crops in Pakistan's Punjab region despite intensification of irrigation. Agric. Water Manage. 281.
Birthal, P.S., Hazrana, J., Negi, D.S., Pandey, G., 2021. Benefits of irrigation against heat stress in agriculture: evidence from wheat crop in India. Agric. Water Manage. 255.
Bradford, J.B., Hicke, J.A., Lauenroth, W.K., 2005. The relative importance of light-use efficiency modifications from environmental conditions and cultivation for estimation of large-scale net primary productivity. Remote Sens. Environ. 96, 246–255.
Bras, T.A., Seixas, J., Carvalhais, N., Jagermeyr, J., 2021. Severity of drought and heatwave crop losses tripled over the last five decades in Europe. Environ. Res. Lett. 16.
Carter, E.K., Melkonian, J., Riha, S.J., Shaw, S.B., 2016. Separating heat stress from moisture stress: analyzing yield response to high temperature in irrigated maize. Environ. Res. Lett. 11.
Chang, Q., Xiao, X., Doughty, R., Wu, X., Jiao, W., Qin, Y., 2021. Assessing variability of optimum air temperature for photosynthesis across site-years, sites and biomes and their effects on photosynthesis estimation. Agr. Forest. Meteorol. 298-299, 108277.
Chen, T., van der Werf, G.R., Gobron, N., Moors, E.J., Dolman, A.J., 2014. Global cropland monthly gross primary production in the year 2000. Biogeosciences. 11, 3871–3880.
Cheng, N., et al., 2023. Exploring light use efficiency models capacities in characterizing environmental impacts on paddy rice productivity. Int. J. Appl. Earth Observat. Geoinform. 117.
Cheng, Y.-B., Zhang, Q., Lyapustin, A.I., Wang, Y., Middleton, E.M., 2014. Impacts of light use efficiency and fPAR parameterization on gross primary production modeling. Agr. Forest. Meteorol. 189-190, 187–197.
Coffel, E.D., Horton, R.M., de Sherbinin, A., 2018. Temperature and humidity based projections of a rapid rise in global heat stress exposure during the 21(st) century. Environ. Res. Lett. 13.
Collatz, G.J., Ball, J.T., Grivet, C., Berry, J.A., 1991. Physiological and environmental regulation of stomatal conductance, photosynthesis and transpiration: a model that includes a laminar boundary layer. Agr. Forest Meteorol. 54, 107–136.
Collatz, G.J., Ribas-Carbó, M., Berry, J.A., 1992. Coupled photosynthesis-stomatal conductance model for leaves of C4 plants. Aust. J. Plant Physiol. 19, 519–538.
Dare-Idowu, O., Brut, A., Cuxart, J., Tallec, T., Rivalland, V., Zawilski, B., et al., 2021. Surface energy balance and flux partitioning of annual crops in southwestern France. Agr. Forest. Meteorol. 308.
De Kauwe, M.G., Medlyn, B.E., Pitman, A.J., Drake, J.E., Ukkola, A., Griebel, A., et al., 2019. Examining the evidence for decoupling between photosynthesis and transpiration during heat extremes. Biogeosciences. 16, 903–916.
Deryng, D., Conway, D., Ramankutty, N., Price, J., Warren, R., 2014. Global crop yield response to extreme heat stress under multiple climate change futures. Environ. Res. Lett. 9, 034011.
Ding, L., Li, Z., Xu, K., Huang, M., Shen, B., Hou, L., et al., 2024. A water stress factor based on normalized difference water index substantially improved the accuracy of light use efficiency model for arid and semi-arid grasslands. J. Environ. Manage. 349, 119566.
Dong, J., Li, L., Shi, H., Chen, X., Luo, G., Yu, Q., 2017. Robustness and Uncertainties of the "Temperature and Greenness" Model for Estimating Terrestrial Gross Primary Production. Sci. Rep. 7, 44046.
Donohue, R.J., Hume, I.H., Roderick, M.L., McVicar, T.R., Beringer, J., Hutley, L.B., et al., 2014. Evaluation of the remote-sensing-based DIFFUSE model for estimating photosynthesis of vegetation. Remote Sens. Environ. 155, 349–365.
Emmel, C., Winkler, A., Hörtnagl, L., Revill, A., Ammann, C., D'Odorico, P., et al., 2018. Integrated management of a Swiss cropland is not sufficient to preserve its soil carbon pool in the long term. Biogeosciences. 15, 5377–5393.
Fensholt, R., Sandholt, I., Rasmussen, M.S., 2004. Evaluation of MODIS LAI, fAPAR and the relation between fAPAR and NDVI in a semi-arid environment using in situ measurements. Remote Sens. Environ. 91, 490–507.
Field, C.B., 1991. 2 - Ecological scaling of carbon gain to stress and resource availability. In: Mooney, H.A., Winner, W.E., Pell, E.J. (Eds.), Response of Plants to Multiple Stresses. Academic Press, San Diego, pp. 35–65.
Fisher, J.B., Tu, K.P., Baldocchi, D.D., 2008. Global estimates of the land–atmosphere water flux based on monthly AVHRR and ISLSCP-II data, validated at 16 FLUXNET sites. Remote Sens. Environ. 112, 901–919.
Garcia, R., Kanemasu, E.T., Blad, B.L., Bauer, A., Hatfield, J.L., Major, D.J., et al., 1988. Interception and use efficiency of light in winter wheat under different nitrogen regimes. Agr. Forest. Meteorol. 44, 175–186.
Gitelson, A.A., Arkebauer, T.J., Suyker, A.E., 2018. Convergence of daily light use efficiency in irrigated and rainfed C3 and C4 crops. Remote Sens. Environ. 217, 30–37.
Gitelson, A.A., Zygielbaum, A.I., Arkebauer, T.J., Walter-Shea, E.A., Solovchenko, A., 2024. Stress detection in vegetation based on remotely sensed light absorption coefficient. Int. J. Remote Sens. 45, 259–277.
Gowik, U., Bräutigam, A., Weber, K.L., Weber, A.P., Westhoff, P., 2011. Evolution of C4 photosynthesis in the genus Flaveria: how many and which genes does it take to make C4? Plant Cell 23, 2087–2105.
He, H., Liu, M., Xiao, X., Ren, X., Zhang, L., Sun, X., et al., 2014. Large-scale estimation and uncertainty analysis of gross primary production in Tibetan alpine grasslands. J. Geophys. Res.: Biogeosciences 119, 466–486.

He, M.Z., Ju, W.M., Zhou, Y.L., Chen, J.M., He, H.L., Wang, S.Q., et al., 2013. Development of a two-leaf light use efficiency model for improving the calculation of terrestrial gross primary productivity. Agr. Forest. Meteorol. 173, 28–39.
Heino, M., Kinnunen, P., Anderson, W., Ray, D.K., Puma, M.J., Varis, O., et al., 2023. Increased probability of hot and dry weather extremes during the growing season threatens global crop yields. Sci. Rep. 13, 3583.
Horn, J.E., Schulz, K., 2011. Identification of a general light use efficiency model for gross primary production. Biogeosciences. 8, 999–1021.
Hwang, Y., Ryu, Y., Huang, Y., Kim, J., Iwata, H., Kang, M., 2020. Comprehensive assessments of carbon dynamics in an intermittently-irrigated rice paddy. Agr. Forest. Meteorol. 285.
Jarvis, A.J., Stauch, V.J., Schulz, K., Young, P.C., 2004. The seasonal temperature dependency of photosynthesis and respiration in two deciduous forests. Global Change Biol 10, 939–950.
Jarvis, P.G., Leverenz, J.W., 1983. Productivity of temperate, deciduous and evergreen forests. In: Lange, O.L., Nobel, P.S., Osmond, C.B., Ziegler, H. (Eds.), Physiological Plant Ecology IV: Ecosystem Processes: Mineral Cycling, Productivity and Man's Influence. Springer Berlin Heidelberg, Berlin, Heidelberg, pp. 233–280.
Jarvis, P.G., Monteith, J.L., Weatherley, P.E., 1997. The interpretation of the variations in leaf water potential and stomatal conductance found in canopies in the field. Philos. Trans. R. Soc. Lond. B, Biol. Sci. 273, 593–610.
Jiang, S., Zhao, L., Liang, C., Cui, N., Gong, D., Wang, Y., et al., 2021. Comparison of satellite-based models for estimating gross primary productivity in agroecosystems. Agr. Forest. Meteorol. 297, 108253.
Jones, J.W., Antle, J.M., Basso, B., Boote, K.J., Conant, R.T., Foster, I., et al., 2017. Toward a new generation of agricultural system data, models, and knowledge products: State of agricultural systems science. Agric. Syst. 155, 269–288.
June, T., Evans, J.R., Farquhar, G.D., 2004. A simple new equation for the reversible temperature dependence of photosynthetic electron transport: a study on soybean leaf. Funct. Plant Biol. 31, 275–283.
Katul, G.G., Palmroth, S., Oren, R.A.M., 2009. Leaf stomatal responses to vapour pressure deficit under current and CO2-enriched atmosphere explained by the economics of gas exchange. Plant, Cell Environ. 32, 968–979.
Lai, P., Marshall, M., Darvishzadeh, R., Tu, K., Nelson, A., 2024. Characterizing crop productivity under heat stress using MODIS data. Agr. Forest. Meteorol. 355, 110116.
Lesk, C., Rowhani, P., Ramankutty, N., 2016. Influence of extreme weather disasters on global crop production. Nature 529, 84–87.
Lesk, C., Anderson, W., Rigden, A., Coast, O., Jägermeyr, J., McDermid, S., et al., 2022. Compound heat and moisture extreme impacts on global crop yields under climate change. Nature Rev. Earth Environ. 3, 872–889.
Li, L., Liangfu, C., Yanhua, G., Qinhuo, L., 2009. A study on GPP inversion of different ecosystems by remote sensing and impact factors comparison. In: 2009 IEEE International Geoscience and Remote Sensing Symposium, IV. -284-IV-287.
Li, S., Xiao, J., Xu, W., Yan, H., 2012. Modelling gross primary production in the Heihe river basin and uncertainty analysis. Int. J. Remote Sens. 33, 836–847.
Liebig, 1841. Organic chemistry in its application to agriculture and physiology. Br. Foreign. Med. Rev. 11, 436–447.
Lilburne, L., Tarantola, S., 2009. Sensitivity analysis of spatial models. Int. J. Geographic. Inf. Sci. 23, 151–168.
Liu, Z., Wu, C., Peng, D., Wang, S., Gonsamo, A., Fang, B., et al., 2017. Improved modeling of gross primary production from a better representation of photosynthetic components in vegetation canopy. Agr. Forest. Meteorol. 233, 222–234.
Liu, Z.H., Hu, M.Q., Hu, Y.M., Wang, G.X., 2018. Estimation of net primary productivity of forests by modified CASA models and remotely sensed data. Int. J. Remote Sens. 39, 1092–1116.
Lobell, D.B., Sibley, A., Ortiz-Monasterio, J.I., 2012. Extreme heat effects on wheat senescence in India. Nat. Clim. Chang. 2, 186–189.
Loubet, B., Laville, P., Lehuger, S., Larmanou, E., Fléchard, C., Mascher, N., et al., 2011. Carbon, nitrogen and Greenhouse gases budgets over a four years crop rotation in northern France. Plant Soil. 343, 109–137.
Lu, Y., Williams, I.N., Bagley, J.E., Torn, M.S., Kueppers, L.M., 2017. Representing winter wheat in the community land model (version 4.5). Geosci. Model Dev. 10, 1873–1888.
Ma, X., Huete, A., Yu, Q., Restrepo-Coupe, N., Beringer, J., Hutley, L.B., et al., 2014. Parameterization of an ecosystem light-use-efficiency model for predicting savanna GPP using MODIS EVI. Remote Sens. Environ. 154, 253–271.
Mäkelä, A., Pulkkinen, M., Kolari, P., Lagergren, F., Berbigier, P., Lindroth, A., et al., 2008. Developing an empirical model of stand GPP with the LUE approach: analysis of eddy covariance data at five contrasting conifer sites in Europe. Global Change Biol 14, 92–108.
Malmstrom, C.M., Thompson, M.V., Juday, G.P., Los, S.O., Randerson, J.T., Field, C.B., 1997. Interannual variation in global-scale net primary production: Testing model estimates. Global. Biogeochem. Cycles. 11, 367–392.
Marshall, M., Haridasan, D., Campomanes, F., 2023. Biogeographic Limits of C4 Engineered Rice. PREPRINT (Version 1). Research Square. https://doi.org/10.21203/rs.3.rs-3333949/v1 available at.
Marshall, M., Tu, K., Brown, J., 2018. Optimizing a remote sensing production efficiency model for macro-scale GPP and yield estimation in agroecosystems. Remote Sens. Environ. 217, 258–271.
Matthews, T., 2018. Humid heat and climate change. Progr. Phys. Geography: Earth Environ. 42, 391–405.
Medlyn, B.E., Duursma, R.A., Eamus, D., Ellsworth, D.S., Prentice, I.C., Barton, C.V.M., et al., 2011. Reconciling the optimal and empirical approaches to modelling stomatal conductance. Glob. Change Biol. 17, 2134–2144.
Meehl, G.A., Tebaldi, C., 2004. More intense, more frequent, and longer lasting heat waves in the 21st century. Science (1979) 305, 994–997.
Meijide, A., Manca, G., Goded, I., Magliulo, V., di Tommasi, P., Seufert, G., et al., 2011. Seasonal trends and environmental controls of methane emissions in a rice paddy field in Northern Italy. Biogeosciences. 8, 3809–3821.
Monteith, J.L., 1969. Light interception and Radiative exchange in crop stands. Physiol. Aspect. Crop. Yield 89–111.
Moore, C.E., Meacham-Hensold, K., Lemonnier, P., Slattery, R.A., Benjamin, C., Bernacchi, C.J., et al., 2021. The effect of increasing temperature on crop photosynthesis: from enzymes to ecosystems. J. Exp. Bot. 72, 2822–2844.
Morgan, J.A., LeCain, D.R., Pendall, E., Blumenthal, D.M., Kimball, B.A., Carrillo, Y., et al., 2011. C4 grasses prosper as carbon dioxide eliminates desiccation in warmed semi-arid grassland. Nature 476, 202–205.
Myneni, R., Yuri, K., Park, T., 2021. MODIS/Aqua leaf area index/FPAR 8-Day L4 Global 500m SIN Grid. NASA EOSDIS Land Processes Distributed Active Archive Center.
Myneni, R.B., Hoffman, S., Knyazikhin, Y., Privette, J.L., Glassy, J., Tian, Y., et al., 2002. Global products of vegetation leaf area and fraction absorbed PAR from year one of MODIS data. Remote Sens. Environ. 83, 214–231.
Olofsson, P., Eklundh, L., 2007. Estimation of absorbed PAR across Scandinavia from satellite measurements. Part II: Modeling and evaluating the fractional absorption. Remote Sens. Environ. 110, 240–251.
Ouyang, Z.T., Jackson, R.B., McNicol, G., Fluet-Chouinard, E., Runkle, B.R.K., Papale, D., et al., 2023. Paddy rice methane emissions across Monsoon Asia. Remote Sens. Environ. 284.
Pastorello, G., Trotta, C., Canfora, E., et al., 2020. The FLUXNET2015 dataset and the ONEFlux processing pipeline for eddy covariance data. Sci. Data 7, 225. https://doi.org/10.1038/s41597-020-0534-3.
Pei, Y., Dong, J., Zhang, Y., Yang, J., Zhang, Y., Jiang, C., et al., 2020. Performance of four state-of-the-art GPP products (VPM, MOD17, BESS and PML) for grasslands in drought years. Ecol. Inform. 56, 101052.
Pei, Y., Dong, J., Zhang, Y., Yuan, W., Doughty, R., Yang, J., et al., 2022. Evolution of light use efficiency models: Improvement, uncertainties, and implications. Agr. Forest. Meteorol. 317, 108905.
Perkins-Kirkpatrick, S.E., Lewis, S.C., 2020. Increasing trends in regional heatwaves. Nat. Commun. 11, 3357.
Perkins, S.E., Alexander, L.V., Nairn, J.R., 2012. Increasing frequency, intensity and duration of observed global heatwaves and warm spells. Geophys. Res. Lett. 39.
Potter, C.S., Randerson, J.T., Field, C.B., Matson, P.A., Vitousek, P.M., Mooney, H.A., et al., 1993. Terrestrial ecosystem production: a process model based on global satellite and surface data. Global. Biogeochem. Cycles. 7, 811–841.
Prasad, P.V.V., Staggenborg, S.A., Ristic, Z., 2008. Impacts of drought and/or heat stress on physiological, developmental, growth, and yield processes of crop plants. Response Crops. Limited Water 301–355.
Prescher, A.-K., Grünwald, T., Bernhofer, C., 2010. Land use regulates carbon budgets in eastern Germany: from NEE to NBP. Agr. Forest. Meteorol. 150, 1016–1025.
Priestley, C.H.B., Taylor, R.J., 1972. On the assessment of surface heat flux and evaporation using large-scale parameters. Mon. Weather. Rev. 100, 81–92.
Prince, S.D., Goward, S.N., 1995. Global primary production: a remote sensing approach. J. Biogeogr. 22, 815–835.
Raich, J.W., Rastetter, E.B., Melillo, J.M., Kicklighter, D.W., Steudler, P.A., Peterson, B. J., et al., 1991. Potential net primary productivity in south-America - application of a global-model. Ecol. Appl. 1, 399–429.
Ranucci, S., Bertolini, T., Vitale, L., Di Tommasi, P., Ottaiano, L., Oliva, M., et al., 2011. The influence of management and environmental variables on soil N2O emissions in a crop system in Southern Italy. Plant Soil. 343, 83–96.
Reichstein, M., Falge, E., Baldocchi, D., Papale, D., Aubinet, M., Berbigier, P., et al., 2005. On the separation of net ecosystem exchange into assimilation and ecosystem respiration: review and improved algorithm. Global Change Biol 11, 1424–1439.
Rezaei, E.E., Webber, H., Gaiser, T., Naab, J., Ewert, F., 2015. Heat stress in cereals: mechanisms and modelling. Eur. J. Agron. 64, 98–113.
Ristic, Z., Bukovnik, U., Momčilović, I., Fu, J., Vara Prasad, P.V., 2008. Heat-induced accumulation of chloroplast protein synthesis elongation factor, EF-Tu, in winter wheat. J. Plant Physiol. 165, 192–202.
Roy, D.P., Borak, J.S., Devadiga, S., Wolfe, R.E., Zheng, M., Descloitres, J., 2002. The MODIS land product quality assessment approach. Remote Sens. Environ. 83, 62–76.
Runkle, B.R.K., Suvoscarev, K., Reba, M.L., Reavis, C.W., Smith, S.F., Chiu, Y.L., et al., 2019. Methane emission reductions from the alternate wetting and drying of rice fields detected using the eddy covariance method. Environ. Sci. Technol. 53, 671–681.
Running, S.W., Nemani, R.R., Heinsch, F.A., Zhao, M., Reeves, M., Hashimoto, H., 2004. A continuous satellite-derived measure of global terrestrial primary production. Bioscience 54, 547–560.
Sadok, W., Lopez, J.R., Smith, K.P., 2021. Transpiration increases under high-temperature stress: potential mechanisms, trade-offs and prospects for crop resilience in a warming world. Plant, Cell Environ. 44, 2102–2116.
Schmidt, M., Reichenau, T.G., Fiener, P., Schneider, K., 2012. The carbon budget of a winter wheat field: an eddy covariance analysis of seasonal and inter-annual variability. Agr. Forest. Meteorol. 165, 114–126.
Shew, A.M., Tack, J.B., Nalley, L.L., Chaminuka, P., 2020. Yield reduction under climate warming varies among wheat cultivars in South Africa. Nat. Commun. 11, 4408.
Sims, D.A., Rahman, A.F., Cordova, V.D., El-Masri, B.Z., Baldocchi, D.D., Bolstad, P.V., et al., 2008. A new model of gross primary productivity for North American ecosystems based solely on the enhanced vegetation index and land surface temperature from MODIS. Remote Sens. Environ. 112, 1633–1646.

Sims, D.A., Rahman, A.F., Cordova, V.D., El-Masri, B.Z., Baldocchi, D.D., Flanagan, L.B., et al., 2006. On the use of MODIS EVI to assess gross primary productivity of North American ecosystems. J. Geophys. Res.: Biogeosciences 111.
Sobol, I.M., 1993. Sensitivity Estimates for Nonlinear Mathematical Models. Math. Modelling Comput. Experiment, 4, pp. 407–414.
Suyker, A.E., Verma, S.B., 2012. Gross primary production and ecosystem respiration of irrigated and rainfed maize-soybean cropping systems over 8 years. Agr. Forest. Meteorol. 165, 12–24.
Suyker, A.E., Verma, S.B., Burba, G.G., Arkebauer, T.J., 2005. Gross primary production and ecosystem respiration of irrigated maize and irrigated soybean during a growing season. Agr. Forest. Meteorol. 131, 180–190.
Tiwari, S., Patel, A., Singh, M., Prasad, S.M, 2020. Chapter 2 - regulation of temperature stress in plants. In: Tripathi, D.K., Pratap Singh, V., Chauhan, D.K., Sharma, S., Prasad, S.M., Dubey, N.K., Ramawat, N. (Eds.), Chapter 2 - regulation of temperature stress in plants. Plant Life Under Changing Environment 25–45.
United Nations, 2015. The Global Sustainable Development Report 2015.
Urban, J., Ingwers, M.W., McGuire, M.A., Teskey, R.O., 2017. Increase in leaf temperature opens stomata and decouples net photosynthesis from stomatal conductance in Pinus taeda and Populus deltoides x nigra. J. Exp. Bot. 68, 1757–1767.
Wu, C., Chen, J.M., Desai, A.R., Hollinger, D.Y., Arain, M.A., Margolis, H.A., et al., 2012. Remote sensing of canopy light use efficiency in temperate and boreal forests of North America using MODIS imagery. Remote Sens. Environ. 118, 60–72.
Xiao, J.F., Chevallier, F., Gomez, C., Guanter, L., Hicke, J.A., Huete, A.R., et al., 2019. Remote sensing of the terrestrial carbon cycle: A review of advances over 50 years. Remote Sens. Environ. 233.
Xiao, X., Hollinger, D., Aber, J., Goltz, M., Davidson, E.A., Zhang, Q., et al., 2004a. Satellite-based modeling of gross primary production in an evergreen needleleaf forest. Remote Sens. Environ. 89, 519–534.
Xiao, X., Zhang, Q., Hollinger, D., Aber, J., Moore Iii, B., 2005. Modeling gross primary production of an evergreen Needleleaf forest using MODIS and climate data. Ecol. Appl. 15, 954–969.
Xiao, X.M., Zhang, Q.Y., Braswell, B., Urbanski, S., Boles, S., Wofsy, S., et al., 2004b. Modeling gross primary production of temperate deciduous broadleaf forest using satellite images and climate data. Remote Sens. Environ. 91, 256–270.
Xin, F., Xiao, X., Zhao, B., Miyata, A., Baldocchi, D., Knox, S., et al., 2017. Modeling gross primary production of paddy rice cropland through analyses of data from CO2 eddy flux tower sites and MODIS images. Remote Sens. Environ. 190, 42–55.
Yasin, M., Ahmad, A., Khaliq, T., Habib-ur-Rahman, M., Niaz, S., Gaiser, T., et al., 2022. Climate change impact uncertainty assessment and adaptations for sustainable maize production using multi-crop and climate models. Environ. Sci. Pollut. Res. 29, 18967–18988.
Yu, W., Li, D., Zheng, H., Yao, X., Zhu, Y., Cao, W., et al., 2024. HIDYM: a high-resolution gross primary productivity and dynamic harvest index based crop yield mapper. Remote Sens. Environ. 311, 114301.
Yuan, W., Cai, W., Xia, J., Chen, J., Liu, S., Dong, W., et al., 2014. Global comparison of light use efficiency models for simulating terrestrial vegetation gross primary production based on the LaThuile database. Agr. Forest. Meteorol. 192-193, 108–120.
Yuan, W., Chen, Y., Xia, J., Dong, W., Magliulo, V., Moors, E., et al., 2016. Estimating crop yield using a satellite-based light use efficiency model. Ecol. Indicators 60, 702–709.
Yuan, W., Liu, S., Zhou, G., Zhou, G., Tieszen, L.L., Baldocchi, D., et al., 2007. Deriving a light use efficiency model from eddy covariance flux data for predicting daily gross primary production across biomes. Agr. Forest. Meteorol. 143, 189–207.
Zhang, L.-X., Zhou, D.-C., Fan, J.-W., Hu, Z.-M., 2015a. Comparison of four light use efficiency models for estimating terrestrial gross primary production. Ecol. Model. 300, 30–39.
Zhang, Y., Song, C., Sun, G., Band, L.E., Noormets, A., Zhang, Q., 2015b. Understanding moisture stress on light use efficiency across terrestrial ecosystems based on global flux and remote-sensing data. J. Geophys. Res.: Biogeosci. 120, 2053–2066.
Zhao, C., Liu, B., Piao, S., Wang, X., Lobell, D.B., Huang, Y., et al., 2017. Temperature increase reduces global yields of major crops in four independent estimates. Proc. Natl. Acad. Sci. 114, 9326–9331.
Zhao, C., Zhu, W., 2023. Uncertainty analysis of intra-module environmental stress parameter design in light use efficiency-based gross primary productivity estimation models. Trans. Earth, Environ. Sustain. 1, 271–290.
Zheng, Y., Zhang, L., Xiao, J.F., Yuan, W.P., Yan, M., Li, T., et al., 2018. Sources of uncertainty in gross primary productivity simulated by light use efficiency models: Model structure, parameters, input data, and spatial resolution. Agr. Forest. Meteorol. 263, 242–257.
Zhu, P., Burney, J., Chang, J., Jin, Z., Mueller, N.D., Xin, Q., et al., 2022. Warming reduces global agricultural production by decreasing cropping frequency and yields. Nat. Clim. Chang. 12, 1016–1023.
Zhu, X.G., Long, S.P., Ort, D.R., 2010. Improving photosynthetic efficiency for greater yield. Annu Rev. Plant Biol. 61, 235–261. Vol 61.